Two modes of inhibitory neuronal shutdown distinctly amplify seizures in humans

AUTHORS

Omar J. Ahmed[1,2,3,4,5,14,15,#], Tibin T. John[1,2,15], Shyam K. Sudhakar[1], Ellen K.W. Brennan[1,2], Alcides Lorenzo Gonzalez[1,2], Jason S. Naftulin[8], Emad Eskandar[9], Joseph R. Madsen[10], G. Rees Cosgrove[11], Andrew S. Blum[12], N. Stevenson Potter[12], George A. Mashour[6,7], Leigh R. Hochberg[8,13], Sydney S. Cash[8,14]

AFFILIATIONS

[1]Dept. of Psychology,
[2]Neuroscience Graduate Program,
[3]Michigan Center for Integrative Research in Critical Care,
[4]Kresge Hearing Research Institute,
[5]Dept. of Biomedical Engineering,
[6]Dept. of Anesthesiology,
[7]Dept. of Neurosurgery,
University of Michigan, Ann Arbor, MI 48109.

[8]Dept. of Neurology,
[9]Dept. of Neurosurgery,
Harvard Medical School and Massachusetts General Hospital, Boston, MA 02114

[10]Dept. of Neurosurgery,
Boston Children's Hospital, Boston, MA 02115

[11]Dept. of Neurosurgery,
Harvard Medical School and Brigham and Women's Hospital, Boston, MA 02115

[12]Dept. of Neurology,
Rhode Island Hospital, Providence, RI 02903

[13]School of Engineering, Brown University, Providence, RI 02912

[14]Co-senior authors
[15]Co-first authors

[#]LEAD CONTACT & CORRESPONDING AUTHOR

Omar J. Ahmed
Mail: Department of Psychology, 530 Church St. University of Michigan, Ann Arbor, MI 48109
Email: ojahmed@umich.edu

KEYWORDS: inhibition, excitation, epilepsy, temporal lobe, mesial temporal sclerosis, neocortical dysplasia, neocortex, local field potential, human, depolarization block, spike and wave, secondary generalization, subthreshold dynamics

ABSTRACT

Inhibitory neurons are critical for normal brain function but dysregulated in disorders such as epilepsy. At least two theories exist for how inhibition may acutely decrease during a seizure: hyperpolarization of fast-spiking (FS) inhibitory neurons by other inhibitory neurons, or depolarization block (DB) of FS neurons resulting in an inability to fire action potentials. Firing rate alone is unable to disambiguate these alternatives. Here, we show that human FS neurons can stop firing due to both hyperpolarization and DB within the same seizure. However, only DB of FS cells is associated with dramatic increases in local seizure amplitude, unobstructed traveling waves, and transient increases in excitatory neuronal firing. This result is independent of seizure etiology or focus. Computational models of DB reproduce the *in vivo* human biophysics. These methods enable intracellular decoding using only extracellular recordings in humans and explain the otherwise ambiguous inhibitory neuronal control of human seizures.

INTRODUCTION

Epilepsy is a debilitating disease affecting some 50 million people worldwide[1,2]. Epileptic seizures are thought to result from an imbalance between excitatory and inhibitory neuronal activity[3]. However, electrographically similar seizures on the macroscopic scale can be driven by mechanistically distinct processes on the cellular and cell-type population scale[4]. Thus, the relative roles of local inhibitory and excitatory networks in driving seizure progression must be elucidated to guide the development of novel treatments for intractable epilepsies and our understanding of their associated seizures. Due to the tremendous technical challenges of recording from individual human neurons and the relative sparsity of inhibitory neurons, the activity of well isolated inhibitory interneurons during seizures is only rarely examined[5,6].

There are several theories, based on slice and whole animal experiments, proposing both insufficient[7–15] and excessive[16–20] inhibition as possible facilitators of epileptic activity, with at least two hypotheses for how inhibition may acutely decrease during a seizure: (1) hyperpolarization of fast-spiking (FS) inhibitory neurons by other inhibitory neurons[21–24], or (2) excessive depolarization of FS neurons that precludes subsequent action potentials due to blockade of voltage-dependent sodium channels[12,14,25,56]. Resolving these two theories necessitates whole cell recordings[26], but it is practically impossible to record the intracellular membrane potential of neurons during human seizures *in vivo.* In this study, we address these challenges by combining (1) large-scale extracellular recordings of human neocortical inhibitory and excitatory neurons during focal seizures with secondary generalization and (2) a novel method of decoding

membrane potential trajectory from extracellular action potentials. We show the remarkable ability of active fast-spiking inhibitory neurons to block epileptic traveling waves in human neocortex, and reveal the dynamical control of human seizures by the subthreshold trajectory of inhibitory neurons.

118 **RESULTS**

119 Patients were implanted with intracranial grid electrodes as part of the clinical process
120 of identifying the precise site of origin of their drug-resistant focal epilepsy (see
121 Materials and Methods). A 4x4 mm NeuroPort microarray (Blackrock Microsystems)
122 was also placed in a region of the neocortex that was expected to be in the resection
123 site (Figure 1a; Extended Data Fig. 1a). Histology of the resected tissue confirmed that
124 the electrodes consistently targeted layers 2/3 of the neocortex (Extended Data Fig. 1b).
125 We used these arrays to simultaneously record the activity of dozens of individual
126 neocortical neurons during both ictal and interictal activity. We then classified the
127 neurons as either fast-spiking (FS) inhibitory interneurons or regular-spiking (RS)
128 excitatory cells using well-established criteria[27,28], including action potential shape
129 (Extended Data Fig. 1c-f). FS cells correspond to the class of parvalbumin-expressing
130 interneurons and represent the largest source of inhibition in the neocortex[29]. The
131 resulting information thus allowed us to differentiate between putative inhibitory and
132 excitatory unit activity patterns during seizure progression in humans.

133

134 A total of 37 FS cells and 539 RS cells were recorded across 4 patients with NeuroPort
135 arrays implanted in the temporal neocortex (see Supplementary Methods for details
136 about each patient). As secondarily generalized seizures first reached the arrays, both
137 FS and RS cells increased their rate of action potentials (Figs. 1, 2, and Extended Data
138 Figs. 2-4). This finding is consistent with what is known about the feedforward
139 recruitment of both inhibition and excitation[25,30]. At the population level, the FS firing
140 rate was significantly higher than RS cells (100,000 bootstrap iterations of label-shuffled

141 peak rate differences; p=0.036). Within 40 seconds of seizure onset, the mean FS firing
142 rate fell rapidly to 0-2 Hz at the same time as local field potential intensity increased
143 dramatically to its highest levels (Figs. 1, 2, and Extended Data Figs. 2-4). Consistently,
144 among the best isolated FS units during the seizure (isolation quality discussed in more
145 detail below and see Methods), 10 out of 15 had at least one nearby RS cell that
146 exhibited the peak of its overall activity several seconds after the dramatic fall in local
147 FS activity and accompanying elevation in local field potential intensity (Figs. 1, 2, and
148 Extended Data Figs. 2-4). Thus, at the population level, FS cells show a cessation of
149 activity near the middle of secondarily generalized seizures accompanied by a dramatic
150 increase in the amplitude of seizure activity. This FS cessation is followed by a transient
151 increase in RS cell firing, presumably because these RS cells are now less inhibited
152 due to the loss of FS firing. The RS population rate eventually also fell to an average of
153 0-3 Hz but with a delay of several seconds following FS cells. At the population level,
154 FS cells (N=37) exhibited significantly earlier cessation times than RS cells (N=539)
155 (Fig. 2g-j, FS cell average cessation occurred 4.6 seconds earlier than RS average
156 cessation; 100,000 bootstrap iterations of label-shuffled time differences; p<0.0001).
157
158 We next compared activity patterns among individual FS cells. Many individual FS cells
159 did not start firing until ~10 seconds into the seizure, often starting to fire robustly only
160 after the RS rate had already increased (Figs. 1, 2, and Extended Data Figs. 2-4). As
161 seen with the population means (Fig. 2g), each individual FS cell dramatically reduced
162 its firing roughly half-way through the seizure (Figs. 1, 2, and Extended Data Figs. 2-4).
163 However, even simultaneously recorded FS cells during a single seizure did not

164 necessarily cease firing at the same time, just as they did not start firing at the same
165 time. Figure 1 shows the activity of two simultaneously recorded FS cells that were
166 separated by a distance of 2.04 mm. FS Cell 1 (Fig. 1a) approached cessation ~35
167 seconds into the seizure, and at ~35 seconds, the amplitude of the LFP next to FS Cell
168 1 increased dramatically, as did the firing rate of nearby RS cells. FS Cell 2 (Fig. 1b)
169 approached cessation ~24 seconds into the seizure, and the LFP amplitude next to FS
170 Cell 2 also increased at ~24 seconds, along with the firing rate of nearby RS cells.
171 Furthermore, when sorting all simultaneously recorded channels during a seizure by the
172 timing of transition to the large amplitude spike-and-wave event phase, a raster plot of
173 all spikes with units sorted in the same order produced a similar sequence of mid-
174 seizure firing time cessations (Fig. 1c&d). Thus, FS cell cessation is correlated with a
175 dramatic increase in the very local intensity of seizures.
176
177 Given changing waveform shapes and noise characteristics during seizures[31], an
178 important methodological question arises of how separable clusters in waveform feature
179 space are from each other and from noise to allow valid unit assignments during this
180 period. To quantitatively assess this isolation quality of feature space clusters over the
181 course of seizures, we employed a modified version of the L_{ratio} metric of cluster
182 separation introduced and validated by Schmitzer-Torbert et al. (2005)[58] (see Methods).
183 Cluster divisions with L_{ratio} less than 0.1 are considered to have a significantly low level
184 of false negative contamination, indicating that drops in firing rate are not caused by
185 over-assigning candidate spikes to noise or other clusters due to changing waveform
186 shapes in these divisions. We consider units whose average contamination level across

187 seizure divisions (dynamic L_{ratio}) is less than 0.1 to be a best-isolated subset[58]. Figure 2
188 shows an example of an FS unit whose waveform shape could be well isolated from
189 noise across the entire seizure despite showing a monotonic decrease in spike
190 amplitude (Fig. 2a-c). The isolation quality of this unit throughout the seizure is
191 demonstrated visually by 2D voltage histograms of these waveforms (Fig. 2d) and is
192 quantitatively captured by its dynamic L_{ratio} being far below threshold in all seizure
193 divisions in which it was active (Fig. 2b). This isolation quality was similarly sustainable
194 throughout the seizure for many RS units (e.g. Extended Data Fig. 5), although at a
195 lower proportion than FS units, with 48.6% of FS units meeting this criterion but only
196 19.8% of RS units. This pattern sustained throughout seizures, with the proportion of
197 well-isolated FS units remaining between 30% and 48% across all 8 seizure divisions
198 and that of RS units remaining between 13% and 19% (Extended Data Fig. 6). The
199 apparent difference in sortability by cell type may be because the frequency content of
200 noise is such that random threshold crossings are more similar in shape and amplitude
201 to the wider waveforms of RS units than to the sharper waveforms of FS units. This
202 suggests that FS cell spikes are inherently more distinguishable from noise in human
203 neocortical recordings even during seizures. We considered the best-isolated subset of
204 units following this quantitative criterion in parallel with all-inclusive analyses of firing
205 rate dynamics in various time divisions of seizures with similar results. In particular,
206 similar temporal profiles by cell type were observed throughout seizures when
207 considering all units or only best-sorted units with an average $L_{ratio} < 0.1$ across all
208 divisions for Patient C (Fig. 2e&f), as well as when comparing average firing rate time
209 courses by cell type across all patients (Fig. 2g&h). Furthermore, the observed time

210 difference between mean RS activity cessation timing and mean FS activity cessation
211 timing remained significantly larger than that expected by random cell-type label
212 reshuffling when considering all units ($p<0.0001$; Fig. 2i), as well as only best-isolated
213 units with maximum $L_{ratio} < 0.1$ ($p<0.005$; Fig. 2j). Thus, FS cell cessation occurs several
214 seconds before RS cell cessation across the population as well as for the very best
215 isolated units.
216
217 The firing profile of individual FS cells and the accompanying changes in the seizure
218 LFP amplitude were remarkably consistent across all secondary generalized focal
219 seizures examined, independent of etiology or focus (Figs. 1, 2, and Extended Data
220 Figs. 2-4). In patients with an etiology of mesial temporal sclerosis, where the seizure
221 started focally in the hippocampus or surrounding medial temporal regions, FS cells in
222 the temporal neocortex consistently stopped firing after the seizure secondarily
223 generalized and spread to the neocortex, leading to accompanying increases in seizure
224 LFP amplitude (Fig. 1a&b). Similarly, in a patient with an etiology of neocortical
225 dysplasia (Patient C) where the seizure originated in the temporal neocortex, several
226 cm from the implanted electrode array, FS cells near the array stopped firing within the
227 first 40 seconds of the seizure spreading to that location (Fig. 2a&b). Again, this
228 coincided with a transition to even larger amplitude spike-wave LFP events.
229
230 The variability in FS cessation times raises the question of how seizure waves travel
231 across the neocortex: is there a wave that slowly moves across the cortex[32] or a series
232 of faster waves that are perhaps altered by the local activity of FS cells[11,30,33]? We found

233 fast traveling LFP waves in all patients that swept across the 4x4 mm microelectrode
234 array within 40 ms, at a speed of ~0.1 m/s, consistent with estimates from slice and
235 computational studies[30,34–36]. There was a dramatic effect of individual FS cell activity:
236 when an FS cell was still firing, it was able to impede and alter epileptic traveling waves
237 (Fig. 3a), preventing the wave from increasing the seizure's LFP amplitude in the vicinity
238 of the FS cell. Once the FS cell activity ceased, traveling waves swept through the
239 entire array, successfully recruiting the area around the now-silent FS cell (Figure 3B).
240 Indeed, once all FS cells had switched off, the path of epileptic traveling waves became
241 far more regular and stereotyped. Thus, human FS inhibitory cells possess a
242 remarkable capability to obstruct and alter the path of epileptic traveling waves. This
243 again points to the importance of FS activity in controlling local neuronal activity and
244 LFP dynamics during local seizure propagation but leaves open the question of what is
245 causing them to stop firing during the seizure.
246
247 There are two ways in which FS cells can stop firing during a seizure: 1) they could be
248 hyperpolarized by inhibition from other inhibitory neurons[22], also known as the
249 disinhibition hypothesis[23]; or 2) they could enter depolarization block and thus become
250 incapable of firing additional action potentials, despite receiving strong excitatory
251 synaptic input[12,14,25,56]. These two scenarios produce very different predictions for how
252 the action potential (AP) amplitude of an FS cell should change during a seizure. In the
253 case of hyperpolarization, the AP amplitude should increase as the firing rate is
254 decreasing. In the case of depolarization block, AP amplitude should decrease before
255 the cell stops firing while its firing rate is also decreasing. To monitor the relative

256 contributions of hyperpolarization and excessive depolarization throughout the seizure
257 in each recorded unit, we therefore devised a novel method that decodes the
258 membrane potential regime of neurons from extracellular spike amplitude data by
259 computing the sign of the correlation between AP amplitude and firing rate in each
260 second of the seizure (Fig. 4a-c; see Methods). Some units first paused their firing due
261 to transient inhibition from other cells, as suggested by strongly negative correlations
262 between AP amplitude and firing rate as firing rate initially decreased (Fig. 4b&h;
263 Extended Data Figs. 7&8). This period corresponded precisely to the time period of
264 increased firing in neighboring FS units (Fig. 4d&j). However, these apparently
265 hyperpolarized units resumed their firing after this pause. Cessation of firing
266 subsequently occurred presumably due to massive depolarization of their membrane
267 potential, as demonstrated by strongly positive correlations of AP amplitude and firing
268 rate as these units stopped firing spikes (Fig. 4b&h). The regimes of negative
269 correlation correspond to a dynamic inhibitory control of local firing rates during the
270 seizure, followed by a regime of positive correlation with decreasing AP amplitudes
271 during the final descent in firing rate, a pattern consistent with what is seen during
272 depolarization block.
273
274 This pattern was also seen on the population level in spiking event-triggered averages
275 of the time course of our predicted membrane potential measure (Fig. 4e). Aligning
276 inferred membrane potential time courses around the time of firing rate pauses
277 (dropping below 30% of peak rate) revealed a large negative deflection for FS cells,
278 indicative of these units being inhibited via hyperpolarization to reduce firing rate at this

279 time (Fig. 4e; n=12; $R_{mean,pause}$=-0.44±0.19 [sem]; less than 0 with $p<10^{-7}$ by bootstrap
280 mean resampling test, n_{sample}=10, $N_{bootstrap}$=50,000). Furthermore, the inferred
281 membrane potential amongst the FS cell population showed that this shift was also
282 widespread (Fig. 4f), with 9 out of 12 (75%) FS units pausing during the negative,
283 hyperpolarized regime during this rate-based event. Aligning inferred membrane
284 potential time courses around the later time of firing rate cessation in units (defined by
285 rate falling below 30% of peak rate for the final time) revealed a large positive deflection
286 for FS cells, indicative of these units entering a regime depolarization block (Fig. 4e;
287 n=26; $R_{mean,cess}$=+0.45±0.12 [sem]; greater than 0 with $p<10^{-7}$ by bootstrap mean
288 resampling test, n_{sample}=20, $N_{bootstrap}$=50,000). Again, the inferred membrane potential
289 amongst the FS cell population showed that this shift was also widespread across units
290 (Fig. 4f), with 20 out of 26 (77%) FS units landing in the positive, over-excited regime.
291 When comparing these values only in units that showed both a pause and cessation to
292 control of heterogeneity amongst different units, the inferred membrane potential was
293 still significantly higher as the unit ceased firing compared to as the unit paused its firing
294 (right-sided Wilcoxon signed rank test; n=12, p=0.0049). Finally, these firing rate
295 descents in FS cell activity were associated with distinct changes in LFP amplitude
296 despite being of the same magnitude (at 30% of peak firing rate) as shown by event-
297 triggered averages in LFP amplitude (Fig. 4e). FS cessation was associated with a
298 larger LFP amplitude than that associated with pausing even amongst cells exhibiting
299 both events (right-sided Wilcoxon signed rank test; n=12, $p<10^{-4}$). Similar results were
300 obtained indicative of significant and widespread overexcitation underlying the cessation
301 of activity in RS units, with 225 out of 331 (68%) RS units with sufficient rate at the time

302 of cessation exhibiting a positive value (Extended Data Fig. 7e; n=331;
303 $R_{mean,cess}$=0.30±0.03 [sem]; greater than 0 with $p<10^{-7}$ by bootstrap mean resampling
304 test, n_{sample}=20, $N_{bootstrap}$=50,000). However, amongst RS cells exhibiting a pause in
305 activity, membrane potential appeared much more heterogenous despite controlling for
306 firing rate at this time, appearing in a bimodal distribution amongst both inhibition and
307 depolarization block that was not significantly different from 0 (Extended Data Fig. 7e&f;
308 n=130; $R_{mean,cess}$=-0.08±0.06 [sem]; greater than 0 with p=0.3782, n_{sample}=10,
309 $N_{bootstrap}$=50,000). This may be because RS cells receive a greater diversity of input
310 magnitudes during seizure progression than do FS cells but succumb to the same, more
311 uniform mechanism underlying depolarization block at firing rate cessation and seizure
312 transition, which we hypothesize is due to increasing potassium concentrations in the
313 extracellular environment shared by all of these cells.
314
315 This sequence of significant hyperpolarization in FS cells followed by large and
316 widespread overexcitation in all cells suggests a consistent membrane potential-based
317 mechanism by which local cortical circuits fight but ultimately succumb to seizure
318 progression. The dynamics in firing rate and action potential amplitude that characterize
319 this mechanism were accurately reproduced in a computational model of the cell
320 membrane incorporating voltage-dependent sodium and potassium conductances
321 (Hodgkin-Huxley formalism) with stochastic background synaptic input. The model
322 reproduced all of the observed mutual dynamics between action potential rate and
323 amplitude during inhibitory (hyperpolarizing) pauses versus depolarization-induced

cessation (Fig. 5), confirming the plausibility of this mechanistic sequence driving unit activity patterns during seizure progression.

DISCUSSION

We have shown that both FS and RS cells are strongly activated during the initial spread of secondarily generalized seizures. The immediate increase in RS rate at seizure onset, in particular, clearly indicates spread of the seizure, and not a failed seizure in what has been called an ictal penumbra, where no initial increases in RS rate appear[32]. Importantly, we have shown that both FS and RS cells can sometimes pause their activity due to hyperpolarization (likely due to inhibition-mediated hyperpolarization from other nearby inhibitory neurons) but stop firing midway through secondarily generalized seizures due to depolarization block. This result is independent of seizure etiology (cortical dysplasia vs. mesial temporal sclerosis) or site of origin (hippocampus vs. neocortex). This suggests that there is an almost complete lack of FS-mediated inhibition towards the end of a human seizure, in contrast to some animal models without loss of inhibition[18]. FS cells are active near the beginning and middle of the seizure, in contrast to computational models placing the loss of inhibitory restraint at seizure onset[37]. Strikingly, this absence of FS inhibitory activity is accompanied by large increases in the amplitude of the seizure's LFP and unimpeded fast traveling waves, as well as a short-lasting increase in RS firing. Thus, these results suggest a more complicated set of dynamics than a monotonic increase or decrease of inhibition and provide further insight into the associated biophysical mechanisms.

The main difference between RS and FS cell firing during the seizures observed here was the significantly earlier cessation of spiking by FS cells, which is consistent with previous results from *in vitro* models of seizure-like events showing increased

351 propensity of FS cells to enter depolarization block compared to pyramidal cells[12,14,25].
352 The reason for this difference in propensity to enter depolarization block has not been
353 established, but these results suggest this difference could represent a primary source
354 of imbalance between excitatory and inhibitory cell activities that allows seizures to
355 propagate and transition to a large amplitude phase in human neocortex. One
356 hypothesis accounting for this difference is that of the differential expression of voltage-
357 gated potassium channel units in FS as opposed to RS cells[38–40] in combination with the
358 elevated extracellular potassium ion levels known to occur in the context of
359 seizures[41,42]. However, there are several intrinsic and network-based properties that are
360 known to differ between FS cells and pyramidal cells and could contribute to this
361 difference, such as intrinsic excitability and the relative strength of feedforward drive[43–
362 46]. The results here suggest that properties responsible for increasing the propensity of
363 FS cells to enter depolarization block relative to RS cells are also those that allow the
364 propagation and exacerbation of seizures in human neocortex. Beyond seizure
365 progression, it is also possible that the lack of FS activity sets in motion a critical
366 network-level transition that leads to seizure termination[47–49]. This transition may include
367 the activation of inhibitory cell types other than FS cells[22,59].
368
369 In summary, FS cells are the largest source of inhibition in the neocortex, and human
370 FS cells approach cessation less than halfway through a seizure, most likely due to
371 depolarization block. This is associated with a dramatic increase of the seizure's local
372 field potential amplitude and a transition to clear spike-and-wave events at a frequency
373 of ~3 Hz. Rhythmic spike-and-wave discharges, when they occur in the motor cortex,

are responsible for the rhythmic ~3 Hz movements seen during the clonic phase of tonic-clonic seizures[50]. Importantly, this suggests a novel, FS-dependent, mechanistic explanation for the two behaviorally defined phases of secondarily generalized tonic-clonic seizures: the high-FS-rate, low-LFP-amplitude phase of the seizure corresponds to the tonic phase, whereas the post-FS-cessation phase with periodic spike-wave bursts corresponds to a longer lasting clonic phase. Thus, in addition to existing approaches[51–55], novel therapies that prevent FS cells from entering depolarization block may prevent - or at least limit the severity of - seizures, representing a novel and potentially powerful avenue for treating seizures with many different etiologies.

385 **METHODS**

386 **Patients & Clinical/Research Electrode Placement**

387 Approval for all experiments was granted by the Institutional Review Boards of
388 Massachusetts General Hospital / Brigham & Women's Hospital and Rhode Island
389 Hospital. The decision to implant intracranial electrodes in an epilepsy patient as well
390 the positioning of those electrodes in a patient was made solely on clinical factors by
391 clinical staff. The explicit goal of this study was to examine the single neuron correlates
392 of tonic-clonic seizures[42] with focal onsets (also referred to as focal seizures with
393 secondary generalization), one of the most common kind of epilepsies[56]. These focal
394 seizures have a localized onset zone, either in the mesial temporal lobe or neocortex,
395 but secondarily generalize, spreading to both hemispheres and almost always leading
396 to impaired consciousness. Here, we studied data from 4 patients (Patients A,B,C,D)
397 with clear focal seizures with secondary generalization, with each of these clinical
398 seizures showing clear spike-and-wave patterns. Two additional patients with temporal-
399 lobe epilepsy were implanted with NeuroPort Arrays but not studied here because one
400 of them did not have any seizures while implanted (Patient E), and the NeuroPort Array
401 in the other patient did not sample any typical spike-and-wave seizures (Patient F). A
402 total of 10 secondarily generalized seizures with spike-and-wave discharges from the 4
403 patients were analyzed (3 each from Patients A and D; 2 each from Patients B and C).
404 A detailed clinical description of each of these 4 patients follows:

405 **Patient A.** Patient A was a left-handed man in his 30s at the time of his surgery. He had
406 suffered from pharmacologically intractable partial complex seizures for almost two
407 decades. His seizures lasted 1-2 minutes and were characterized by a sudden onset of

408 slurred and nonsensical speech. This was followed by a staring spell, lack of
409 responsiveness, and head turning to the right. He also displayed automatisms and
410 posturing that involved his right arm and hand more than his left. MRI suggested left
411 (dominant) temporal polymicrogyria. He underwent placement of grids and strips for ~2
412 weeks to delineate the seizure focus with respect to this area of abnormal sulcation. A
413 4x4 mm NeuroPort array with 1.5 mm long contacts was placed in the left superior
414 temporal gyrus. Seizures were found to emanate from the mesial temporal structures,
415 but during secondary generalization, the seizures spread to the location of the array in
416 the superior temporal gyrus and beyond. The patient underwent a left temporal
417 lobectomy, and histology confirmed that the microarray targeted layer 3. Pathology was
418 consistent with mesial temporal sclerosis.
419
420 **Patient B.** Patient B was a right-handed man in his 40s at the time of his surgery, with a
421 history of medically refractory epilepsy. His seizures lasted 1-2 minutes. Clinically, the
422 seizures started with arousal and bilateral arm and leg extension. This was followed by
423 leftward head deviation, left arm flexion, and generalized tonic-clonic activity. He
424 underwent placement of grids, strips, and depths in his right hemisphere. A 4x4 mm
425 NeuroPort array (with 1.5 mm deep contacts) was placed in the right middle temporal
426 gyrus. During secondary generalization, the seizures spread to the location of the
427 NeuroPort array in the middle temporal gyrus and beyond. The patient underwent a
428 right temporal lobectomy. Histology on the resected tissue confirmed that the microarray
429 targeted layer 3.
430

431 **Patient C.** Patient C was a left-handed woman in her 20s at the time of her surgery.
432 She started to have complex partial seizures at least 10 years prior to surgery. These
433 seizures included an aura of nausea and a 'tunneling' sensation, then a flattening of
434 affect, slowed responsiveness, automatisms, and associated amnesia. Such seizures
435 occurred 3-4 times per month and were persistent despite being on a three-drug
436 anticonvulsant regimen. MRI revealed an extensive nodular gray matter heterotopia in
437 the right hemisphere. Video-EEG monitoring had found right hemispheric onset
438 seizures, and fMRI had shown normal left sided language activation patterns and
439 normal motor activation patterns. Wada testing confirmed left hemispheric language
440 dominance and suggested her left hemisphere could adequately support memory
441 function subsequent to a right temporal lobectomy. Based on these data, she was
442 implanted with a combination of subdural grid and strip electrodes over the right
443 hemisphere and 3 depth electrodes into the right temporal lobe. The NeuroPort array
444 (with 1.5 mm deep contacts) was placed in the right middle temporal gyrus. Her
445 seizures lasted between 1-2.5 minutes. These showed very consistent patterns of
446 seizure onset and propagation on ECoG; all began in the right middle and upper gyri of
447 the posterior temporal cortex. Low amplitude and fast activity were recorded from these
448 grid sites at the onset, followed by a buildup of 11-13 Hz activities from these leads
449 which then spread anteriorly and inferiorly along the grid. Rhythmic spike-wave
450 discharges were also detected soon after seizure onset spreading to several locations,
451 including the location of the NeuroPort array in the right middle temporal gyrus. The
452 patient underwent an extensive right temporal resection with extension posteriorly
453 toward the right temporo-occipital junction but sparing of much of the mesial temporal

454 structures (including the hippocampus). Histology confirmed that the array targeted
455 layers 2/3. Pathology revealed subtle neuronal dysgenesis and focal superficial gliosis
456 and encephalomalacia in the posterior temporal neocortex, including the recorded
457 seizure-onset zone. Anterior temporal cortex showed mild gliosis.
458
459 **Patient D.** Patient D was a right-handed man in his 20s whose seizures began when he
460 was a teenager. His seizures were characterized by a blank stare and oral automatisms
461 accompanied by stiffening and posturing of the right hand. His MRI was unremarkable,
462 but his semiology and phase I EEG recordings suggested a left temporal seizure onset.
463 Consequently, he was implanted with several strip electrodes covering the left frontal
464 and temporal regions. The NeuroPort array (1.0 mm deep contacts) was placed in the
465 middle temporal gyrus about 1–2 cm posterior to the temporal tip. All of the seizures
466 had similar clinical and electrographic signatures with a left gaze preference at onset
467 followed by tonic and then clonic movements of the right arm. Electrographically, the
468 seizures began with a generalized burst of sharp waves followed by sharp wave com-
469 plexes that were maximal in mesial temporal leads. The participant underwent a left
470 temporal lobectomy. Histological examination of the tissue revealed mild dysplastic
471 changes in the lateral temporal neocortex and gliosis and moderate neuronal loss in
472 regions CA4 and CA3 of the hippocampus.
473
474 **NeuroPort Recordings, Data Collection & Analysis**
475 A Neuroport array (manufactured by Blackrock Microsystems) is a 10x10 grid of
476 electrodes with an inter-electrode spacing of 400 um, giving a total size of 4x4 mm. The

477 depth of the electrodes used in this study was either 1.5 mm (Patients A,B,C) or 1.0 mm
478 (Patient D). 96 of the 100 electrodes were used to record the activity of individual
479 neurons as well as the local field potential (LFP). The 0.3-7500 Hz wideband analog
480 signal from each electrode was referenced to a distant intracranial reference wire and
481 sampled at 30 kHz. The LFP shown in Figs. 1, 2, and Extended Data Fig. 1 were z-
482 scored, but not filtered any further. Traveling wave analysis & images (Fig. 3) made use
483 of these z-scored, unfiltered LFP signals. For single unit analysis, the broadband signal
484 was high-pass filtered above 250 Hz using a 6-pole Bessel filter and then manually
485 spike-sorted using Plexon Offline Sorter. We then classified the neurons as either fast-
486 spiking (FS) inhibitory interneurons or regular-spiking (RS) excitatory cells using well-
487 established criteria[27,28], including action potential shape. Cessation of firing during a
488 seizure was defined as the bin after which the firing rate never exceeded 30% of the
489 unit's peak rate. For action-potential (AP) amplitude analysis (Fig. 4a), the AP amplitude
490 was defined as the trough-to-peak amplitude of each individual extracellular action
491 potential.

492

493 **Cluster isolation quality assessment: Dynamic L_{Ratio}**

494 To assess the isolation quality of feature space clusters over the course of seizures, we
495 employed a modified version of the L_{ratio} metric of cluster separation introduced and
496 validated by Schmitzer-Torbert et al. (2005)[58]. This involved first calculating the
497 Mahalanobis distance of every spike to a given cluster's center in a 4D feature space
498 consisting of trough-to-peak amplitude, trough-to-peak width, principal component 1,
499 and principal component 2. The Mahalanobis distance normalizes the Euclidean

500 distance by the variance of a given cluster along its major dimensions to correct for
501 correlations amongst features. Schmitzer-Torbert et al. (2005)[58] showed strong error
502 rate correlation with ground truth extracellular spikes by assuming a multi-dimensional
503 Gaussian distribution for a given cluster and taking the amount of contamination by
504 false negative assignments to be the sum of probabilities of each un-clustered spike of
505 a given Mahalanobis distance to belong to that Gaussian, which was robust to the
506 particular feature space used. These probabilities are given by the inverse of the
507 cumulative distribution function of a chi-squared distribution with degrees of freedom
508 equal to the number of features in the features space, the sum of which is called L.
509 Because clusters in this space moved over the course of the seizure in a non-monotonic
510 pattern here, we calculated Mahalanobis distances to a surrogate cluster for multiple
511 subsets of the whole cluster at 8 equal divisions over the course of the seizure and 3
512 divisions of the 10 minute period that occurred two minutes after the end of the seizure.
513 A composite cluster across initial divisions was used to provide a liberal estimate of the
514 space that a given cluster might occupy despite early waveform shape changes. This
515 composite reference cluster included all available spikes before the seizure along with
516 those in the first two divisions of the seizure, which were generally well-sortable. We
517 calculated the sum of false negative assignment probabilities under a Gaussian model
518 for this reference cluster, the value L, for each seizure and post-seizure division. We
519 then dynamically normalized L by the number of spikes assigned to the cluster in each
520 time division to estimate contamination rates relative to the number of spikes assigned
521 during that division, which we refer to as the dynamic L_{ratio}.
522

523 **Membrane potential trajectory analysis**

524 We exploited the biophysical relationship between depolarization, voltage-gated Na+
525 channel inactivation, and spike waveform shape[60] to infer the direction of membrane
526 potential changes underlying the changes in firing rate exhibited by single units
527 recorded extracellularly in patients across time. This was done for a given unit by first
528 computing the local spike rate and average trough-to-peak waveform amplitude in
529 moving time windows of width 1 second unless otherwise specified, moving with a step
530 size of 0.1 seconds. Then a linear regression was performed at each point in this series
531 across a moving time window of 3 seconds, producing a time series of correlation
532 coefficients for bins with an average spike rate of at least 5 Hz. Strong negative
533 correlations were taken as evidence of firing rate changes associated with membrane
534 potential changes near resting membrane potential, while strong positive correlations
535 were taken as evidence of membrane potential changes closer to firing threshold, near
536 the regime of depolarization block[56].

537

538 **Computational model**

539 Computer simulations of transmembrane voltage dynamics consistent with the
540 extracellular observations here were made in MATLAB R2017b to explore plausible
541 underlying biophysical mechanisms. A 4-dimensional ordinary differential equation
542 model of a patch of neural membrane following the Hodgkin-Huxley formalism of
543 passive (g_L=0.033 mS/cm^2, E_L=-60 mV, $I_L=g_L(V-E_L)$) and voltage-dependent spiking Na+
544 (g_{Na}=60.0 mS/cm^2, E_{Na}=+58 mV, $I_{Na}=g_{Na}m^3h(V-E_{Na})$) and K+ ($g_K$=5 mS/cm^2, E_K=-85
545 mV, $I_K=g_Kn^4(V-E_K)$) conductances was solved using Euler integration with a timestep of

546 0.005 msec. First order kinetics of gating variables *m*, *h*, and *n* were modeled as in
547 previously established models of this form[57]. Slowly changing net synaptic input and
548 extracellular ion gradient changes were considered to constitute a net external drive
549 modeled as an injected inward current. This current follows a temporal form
550 hypothesized to drive human neocortical neurons during secondarily generalized
551 seizures based on the dynamic membrane potential decoding analysis performed here.
552 Fast synaptic inputs were modeled as conductances with a maximum conductance
553 g_{syn}=0.15 mS/cm^2 and an exponential decay time course of 5 milliseconds gated by
554 input spike times generated by a Poisson process with a linearly increasing rate
555 parameter from 0.001 to 0.2 Hz representing increasing input firing rates across seizure.
556 Analysis of the resulting spike trains was completed in the same manner as dynamic
557 membrane potential trajectory decoding was performed for the observed extracellular
558 data.

559

560 **Statistical analyses**

561 In performing hypothesis testing on various metrics describing activity amongst FS and
562 RS units including peak firing rate difference, mean cessation time difference, and mean
563 correlation between spike firing rate and action potential amplitude at time of cessation,
564 we employed bootstrap-based methods to quantify the uncertainty in these metrics. For
565 peak firing rate and cessation time differences this involved combining all relevant unit
566 measurements into a single population, randomly reshuffling RS and FS labels amongst
567 this population, and recomputing the relevant difference metrics $N_{bootstrap}$ times as
568 indicated to generate a distribution of the metric for random unit classifications. The

probability of a Type-I (false positive) error, the p-value, was then reported as the area under the distribution corresponding to values more extreme than the observed value for the original data. For testing the positivity of the mean correlation between spike firing rate and action potential amplitude at time of cessation, this involved first removing correlation coefficients in the time series corresponding to a linear regressions involving spike rates of less than 5 Hz. Then the coefficients at each unit's detected cessation time were resampled with replacement in 20 unit subpopulations 50,000 times (unless otherwise specified) and averaged to generate a bootstrapped sample mean distribution characterizing the variability in this mean relative to zero. The probability of a Type-I (false positive) error that the observed mean coefficient was greater than zero by chance, the p-value, was then reported as the area under the distribution corresponding to values equal to or less than zero. To nonparametrically test the significance of differences in paired measures at cessation and pause times within single units, we employed the right-sided Wilcoxon signed rank test (RMatlab2017b).

Extended Data / Supplementary Information

9 Extended Data Figures (+ legends) are included.

589 **ACKNOWLEDGEMENTS**
590
599 We would like to thank the patient volunteers. This work was supported by the American
600 Epilepsy Society Junior Investigator Research Award, CURE Epilepsy Taking Flight
601 Award, NINDS F32-NS083208 and University of Michigan Startup Funds (OJA), NIH
602 R01-NS062092 (SSC) and NSF graduate student fellowships (TTJ & EKWB).

603

604 **FIGURES AND FIGURE LEGENDS**

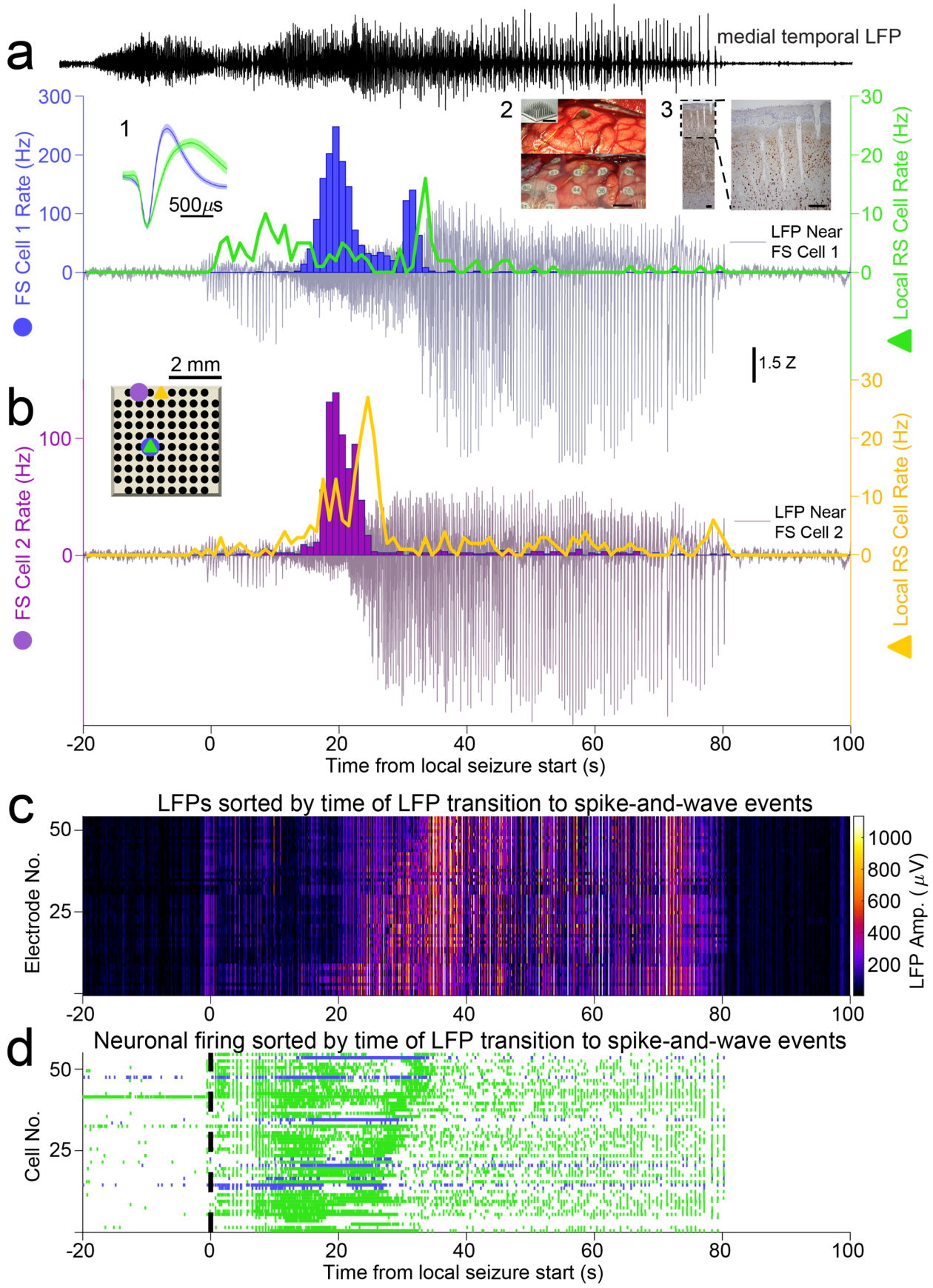
a
medial temporal LFP
FS Cell 1 Rate (Hz)
Local RS Cell Rate (Hz)
1
500μs
2
3
LFP Near
FS Cell 1
1.5 Z
b
2 mm
FS Cell 2 Rate (Hz)
Local RS Cell Rate (Hz)
LFP Near
FS Cell 2
Time from local seizure start (s)
c
LFPs sorted by time of LFP transition to spike-and-wave events
Electrode No.
LFP Amp. (μV)
d
Neuronal firing sorted by time of LFP transition to spike-and-wave events
Cell No.
Time from local seizure start (s)

605

606 **Figure 1: Human neocortical inhibitory and excitatory neurons have different temporal profiles**
607 **relative to secondarily generalized focal seizure progression on local electrodes**
608
609 **a.** ***Upper.*** Electrocorticogram trace (ECoG, black) from contact closest to source of focal seizure in
610 hippocampus of Patient A. Note its time of initiation at T = -20 seconds, substantially preceding
611 the start of the seizure in neocortex. ***Lower.*** The firing rate of a single FS cell (blue), the firing
612 rate of a single RS cell recorded from the same electrode (green) and the local field potential
613 (LFP, gray, recorded from the same electrode as the FS cell) during a seizure recorded from
614 Patient A. Note the decrease in LFP amplitude as the FS cell starts firing, followed by a dramatic
615 increase in LFP seizure amplitude after the FS cell decreases its rate at T=35 seconds. RS cell
616 quickly increases its firing rate as the seizure first spreads to the NeuroPort array (T=0 seconds),
617 then decreases in rate slightly as the FS cell switches on, and finally settles into a lower firing rate
618 regime during the large spike-and-wave events that dominates the remainder of the seizure after
619 FS cell cessation. Inset shows the mean normalized extracellular action potential waveforms (with
620 99% confidence intervals in lighter shading) of FS Cell 1 (blue) and the neighboring RS cell
621 (green). Inset 1: the mean normalized extracellular action potential waveforms (with 99%
622 confidence intervals in lighter shading) of FS Cell 1 (blue) and the neighboring RS cell (green).
623 Inset 2: The implanted microelectrode array (Top) with overlaid clinical grid electrodes (Bottom);
624 Scale bar: 1 cm. Top left corner shows the array before implantation. Scale bar: 200 μm. Inset 3:
625 Histology of resected tissue showing the NeuN-stained neurons in the full neocortical column and
626 electrode tracts and an enlarged image (Right) showing that the array targeted layer 3 of the
627 neocortex. Scale bars: 400 μm.
628
629 **b.** The inset shows a schematic of the array and the location of two simultaneously recorded FS
630 cells separated by ~2 mm: FS Cell 1 (blue, firing rate shown in Fig. **1c**) and FS Cell 2 (purple). FS
631 Cell 2 approached cessation at T=24 seconds, well before FS Cell 1. The LFP (grayish-purple)
632 recorded at the same location as FS Cell 2 dramatically increases at the same time as FS Cell 2
633 decreases firing, well before the increase seen in the LFP recorded next to FS Cell 1. These
634 suggest the activity of FS cells during human seizures is strongly correlated to the local intensity
635 of seizure waves. FS Cell 2 activity cessation again precedes a sharp increase in local RS cell
636 activity (gold), further suggesting an important role of FS cells in controlling local activity during
637 seizure progression.
638
639 **c.** Heatmap shows local LFP amplitude (absolute value) over time on each electrode in NeuroPort
640 array exhibiting classifiable units as each row, sorted by time of start of spike-and-wave event
641 and with brighter colors indicating larger amplitudes. Note the increasing delay to start of spike-
642 and-wave event suggesting different dynamics to seizure spread across the array over the
643 timecourse of approximately 20 seconds.
644
645 **d.** Raster plot showing spike times of all cells on NeuroPort array in Patient A that could be
646 classified into FS (blue) or RS (green) categories with rows sorted by the same order as in (C).
647 Note the increasing delay to reduction in spike density corresponding to LFP transition to spike-
648 and-wave events suggesting control of local seizure progression by local cellular spiking activity.
649

650

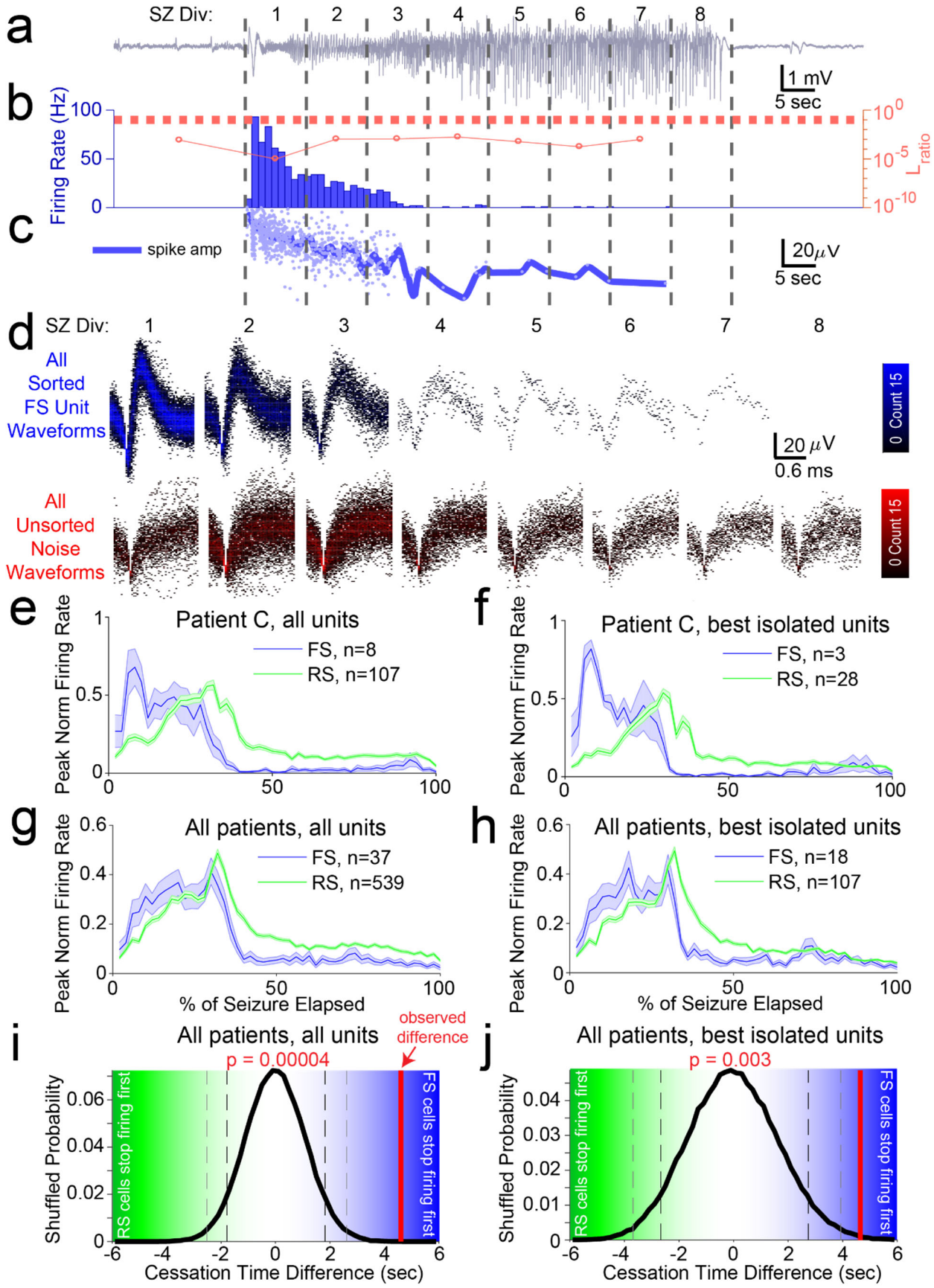
a
SZ Div: 1 2 3 4 5 6 7 8
1 mV
5 sec
b
Firing Rate (Hz)
100
50
0
10^0
10^{-5}
10^{-10}
L_{ratio}
c
spike amp
20 μV
5 sec
d
SZ Div: 1 2 3 4 5 6 7 8
All Sorted FS Unit Waveforms
20 μV
0.6 ms
0 Count 15
All Unsorted Noise Waveforms
0 Count 15
e
Patient C, all units
FS, n=8
RS, n=107
Peak Norm Firing Rate
f
Patient C, best isolated units
FS, n=3
RS, n=28
Peak Norm Firing Rate
g
All patients, all units
FS, n=37
RS, n=539
Peak Norm Firing Rate
% of Seizure Elapsed
h
All patients, best isolated units
FS, n=18
RS, n=107
Peak Norm Firing Rate
% of Seizure Elapsed
i
All patients, all units
observed difference
p = 0.00004
Shuffled Probability
RS cells stop firing first
FS cells stop firing first
Cessation Time Difference (sec)
j
All patients, best isolated units
p = 0.003
Shuffled Probability
RS cells stop firing first
FS cells stop firing first
Cessation Time Difference (sec)

651

Figure 2: Analyzing unit subpopulations by isolation quality demonstrates consistent cell-type specific activity profiles and cessation order despite changing unit amplitude and noise structure.

a. LFP in Patient C indicating seizure as split into 8 equal time divisions for analysis of unit isolation quality across duration of seizure.

b. Bar graph shows firing rate in 1 second bins of best-isolated example FS unit (blue) in Patient C. Dotted red line indicates threshold used to determine best-isolated units using the dynamic L_{ratio} measure (see Methods) in each time division of seizure. Line plot indicates dynamic L_{ratio} in each division (red) and shows large separation of example FS unit from noise in feature space used for clustering throughout the seizure (note log scale).

c. Line plot showing average spike amplitude (dark blue) and individual spike amplitudes (light blue) of example FS unit over course of seizure in Patient C. Note that even as amplitude decreases the unit remains well-isolated from noise as quantified by dynamic L_{ratio} across seizure.

d. Time-voltage histogram of all threshold crossings assigned to this example FS unit (blue, *Upper)* and to noise (red, *Lower*) in eight divisions of seizure in Patient C. Shows unit waveforms are visually distinguishable from threshold crossings assigned as noise across seizure.

e. Average firing rate traces across seizures for each cell type group in Patient C, with y-axis normalized to firing rate peak and x-axis normalized to total seizure duration before averaging. Note right-shifted rate profile of RS units over course of seizure as compared to FS units.

f. Average firing rate traces across seizures for each cell type group using only best-isolated units (see Methods) in Patient C, with y-axis normalized to firing rate peak and x-axis normalized to total seizure duration before averaging. Note right-shifted rate profile of best-isolated RS units over course of seizure as compared to best-isolated FS units.

g. Average firing rate traces across seizures for each cell type group across all patients, with y-axis normalized to firing rate peak and x-axis normalized to total seizure duration before averaging. Note right-shifted rate profile of RS units over course of seizure as compared to FS units.

h. Average firing rate traces across seizures for each cell type group using only best-isolated units (see Methods) across all patients, with y-axis normalized to firing rate peak and x-axis normalized to total seizure duration before averaging. Note right-shifted rate profile of best-isolated RS-classified units over course of seizure as compared to best-isolated FS-classified units.

i. Observed time difference (solid red line) between mean RS activity cessation timing (n=399) and mean FS activity cessation timing (n=37) in relation to probability distribution of this timing difference across random label reshufflings of unit cell type labels ($N_{shuffles}$=100,000; solid black line). P-value indicates probability of observing a value equal to or more extreme than the observed value simply by random assignment of cell type to each unit. Values on the right half correspond to a positive difference between RS and FS cessation, with larger values associated with increasing certainty that FS cells stop firing before RS cells. Values on the left half correspond to a negative difference between RS and FS cessation times, with larger values associated with increasing certainty that RS cells stop firing before FS cells.

j. Observed time difference (solid red line) between mean best-isolated RS activity cessation timing (n=83; Lratio < 0.1 during middle 3 seizure divisions) and mean best-isolated FS activity cessation timing (n=17; Lratio < 0.1 during middle 3 seizure divisions) in relation to probability distribution of this timing difference across random label reshufflings of unit cell type labels ($N_{shuffles}$=100,000; solid black line). P-value indicates probability of observing a value equal to or more extreme than the observed value simply by random assignment of cell type to each unit. Values on the right half correspond to a positive difference between best-isolated RS and best-isolated FS cessation times, with larger values associated with increasing certainty that best-

isolated FS cells stop firing before best-isolated RS cells. Values on the left half correspond to a negative difference between best-isolated RS and best-isolated FS cessation, with larger values associated with increasing certainty that best-isolated RS cells stop firing before best-isolated FS cells.

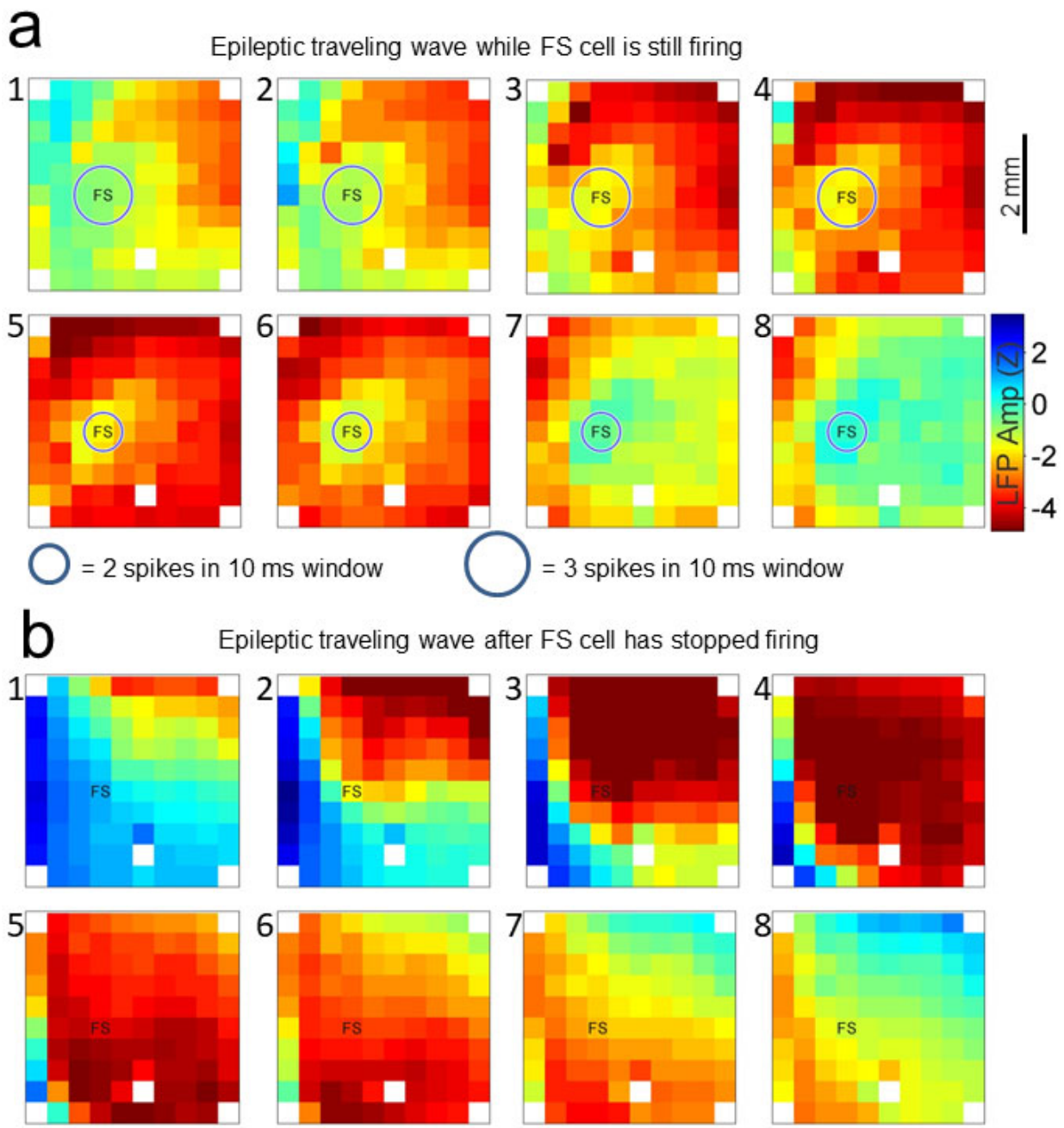

Figure 3: Fast-spiking inhibitory neurons, when still firing, impede the spread of epileptic traveling waves.

a. An example of a traveling wave recorded 30 seconds after the start of a seizure in Patient A. The FS cell located at the position marked “FS” was firing at high rates at this time. The 8 snapshots (1-8) are taken over a 35 ms interval as the traveling LFP wave starts in the top-right corner of the array and travels across the array. The traveling wave does not fully invade the region of neocortex containing the active FS cell, resulting in lower amplitude LFPs around the FS cell. In each subfigure, each square denotes a single LFP sensor, and white squares indicate omitted sensors.

b. An example of a traveling wave recorded 49 seconds after the start of the same seizure. In the absence of FS cell firing, the epileptic traveling wave moves unimpeded through the array, fully invading the region around the marked FS cell and resulting in larger amplitude LFPs at all locations.

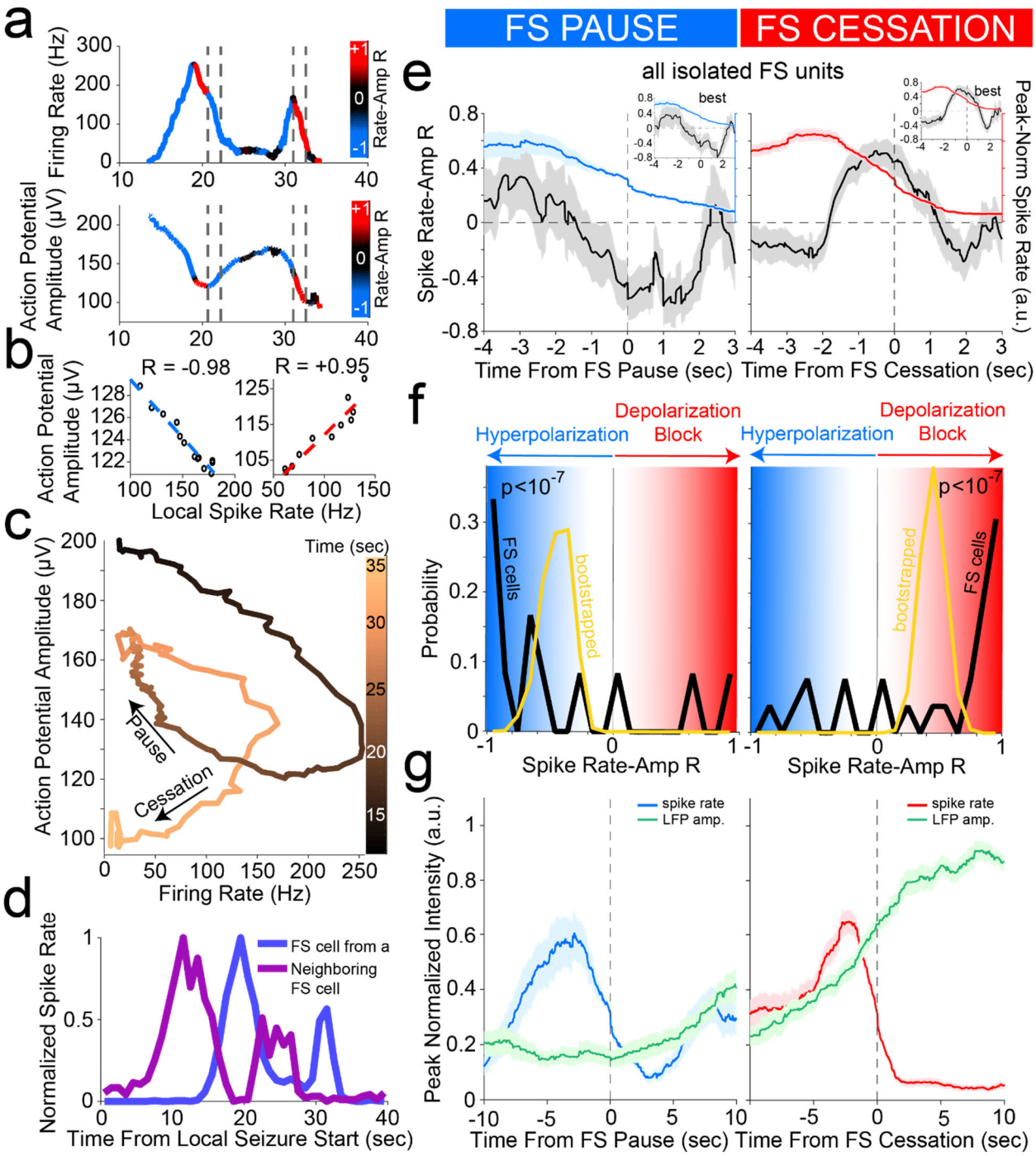

Figure 4. Cessation of individual FS unit activity is consistently associated with inferred membrane potential signatures of depolarization block, despite prior hyperpolarized pauses

a. Firing rate *(upper)* and trough-to-peak spike amplitude (*lower*) of example FS unit in Patient A, color-coded by the local correlation between spike rate and amplitude (in 1 second time bins) as an extracellular proxy for membrane potential trajectory and subthreshold input history. Dotted lines indicate starts and ends of two time periods of firing rate suppression characterized by different membrane potential signatures further characterized in (B), namely a negative correlation regime corresponding to inhibition followed by a positive correlation regime

corresponding to over-excitation ending in firing rate cessation putatively though depolarization block.

b. Example of negative correlation (*left*) between local spike rate and amplitude in first time period indicated by dotted lines in (A) and example of positive correlation (*right*) between local spike rate and amplitude in second time period indicated by dotted lines in (A). Least squares linear fit indicated in dotted lines following color scheme in (A) with Pearson's correlation coefficient indicated above each plot.

c. Trajectory of unit activity over time during seizure in local spike rate vs spike amplitude space, with increasing time indicated by increasingly lighter copper color. The first time period of firing rate reduction in dotted lines in (A) is indicated with an arrow as "Pause" and the second time period of firing rate reduction in dotted lines in (A) is indicated with an arrow as "Cessation."

d. Firing rate of unit from (A) with neighboring FS unit firing rate overlaid, giving further evidence that first period of firing rate suppression corresponds to inhibition from local FS units while second period of firing rate suppression does not correspond to inhibition from local FS units.

e. Unit cessation-triggered population average of the time course of novel membrane potential regime measure, i.e. the correlation coefficient relating spiking amplitude and rate in a local time window, around the two significant descents in firing rate (below 30% of peak rate) that occur in sequence during seizure. These are designated as pause (*left panel*) and cessation (*right panel*). Left panel shows population average firing rate (blue) and inferred membrane potential regime (black) aligned according to the time of pause in each unit, for all FS units displaying a pause (n=14), with inset showing average for best-isolated FS units displaying a pause (n=10). Right panel shows population average firing rate (red) and inferred membrane potential regime (black) aligned according to the cessation time of each unit, for all FS units (n=37), with inset showing average for best-isolated FS units (n=24).

f. Probability distribution of membrane potential regime measure (spike rate-amplitude correlation; black line) at the time of pause (*left panel*) for FS unit pausing subpopulation (n=14) with sample mean distribution (gold line; resampling size n=10, $N_{bootstrap}$=50,000) showing the mean correlation to be significantly below zero, i.e. in the hyperpolarized membrane potential regime (blue). In combination with its declining firing rate, this is indicative of widespread inhibition across this subpopulation at the time of pause. The population distribution of inferred membrane potential regime is also shown at the time of cessation (*right panel*) for the full FS unit population (n=37) with sample mean distribution (gold line; resampling size n=10, $N_{bootstrap}$=50,000) showing the mean correlation to be significantly above zero, i.e. in the highly depolarized membrane potential regime (red). This is indicative of widespread depolarization block occurring across FS population at the time of cessation.

g. Unit cessation-triggered population average of the time course of same-electrode LFP amplitude around unit activity pause (*left panel*) and cessation (*right panel*). In particular, left panel shows population average firing rate (blue) and LFP amplitude (black) aligned according to the time of pause in each unit, for all FS units displaying a pause (n=14). Right panel shows population average firing rate (red) and LFP amplitude (black) aligned according to the time of cessation in each unit, for all FS units (n=37), indicative of larger LFP increase associated with second FS firing rate descent (cessation) than with first (pause) despite comparable local firing rates in the two conditions.

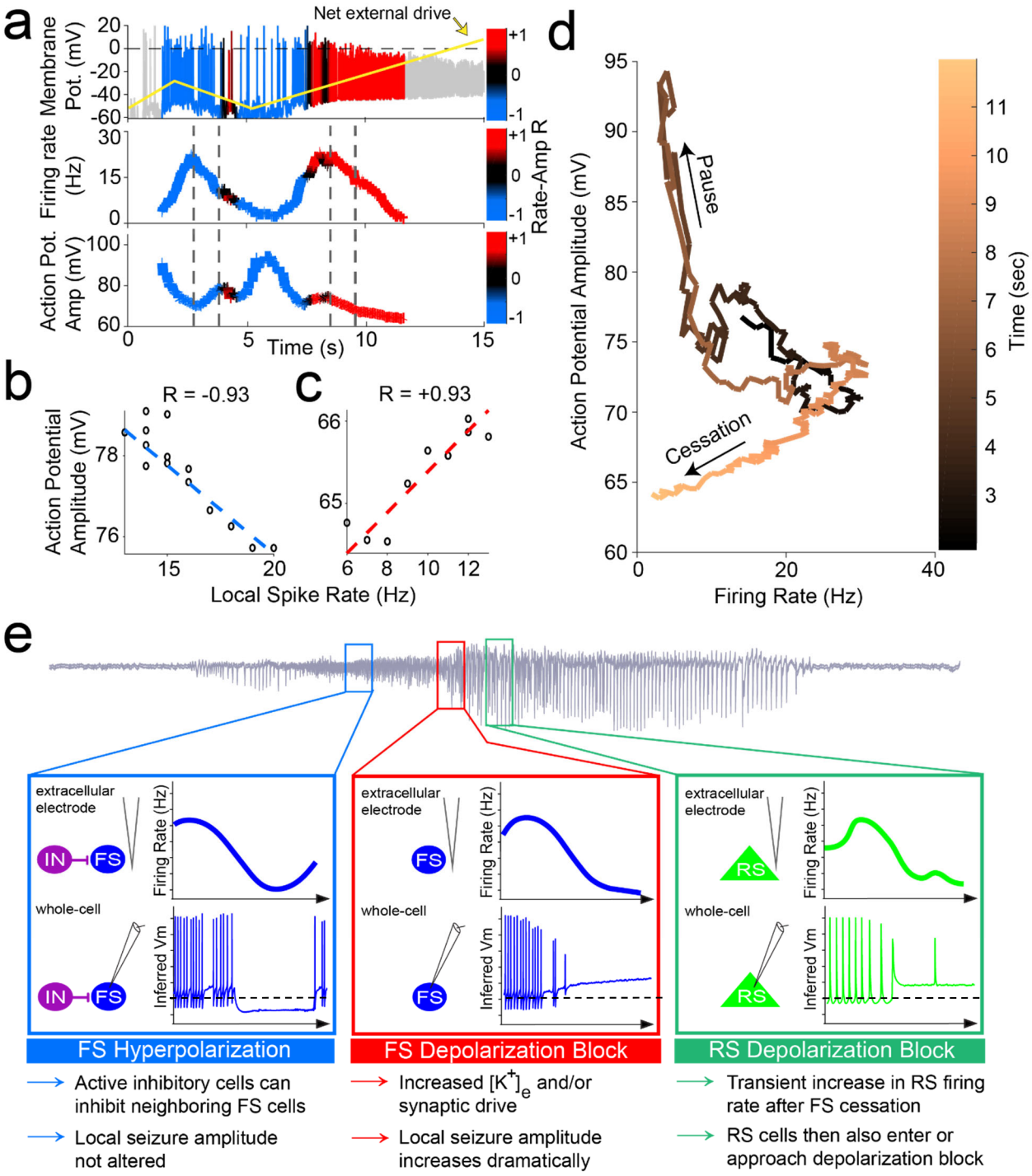

Figure 5. Mechanistic model of unit dynamics across seizure progression: inhibition followed by over-excitation in conductance-based neuron model reproduces key features of extracellular unit behavior during seizures.

a. Simulated membrane potential in conductance-based spiking model color-coded by the local correlation between spike rate and amplitude and with net excitatory input indicated by dotted line. Shows what is hypothesized to be happening within cortical cells during seizure progression as inferred from extracellular spike shape and rate dynamics.

b. Firing rate *(upper)* and trough-to-peak spike amplitude (*lower*) of example FS unit in Patient A, color-coded by the local correlation between spike rate and amplitude as an extracellular proxy for membrane potential and subthreshold input history. Dotted lines indicate starts and ends of two time periods of firing rate suppression characterized by different membrane potential signatures further characterized in (B), namely a negative correlation regime corresponding to inhibition followed by a positive correlation regime corresponding to over-excitation ending in firing rate cessation putatively though depolarization block.

c. Example of negative correlation (*left*) between local spike rate and amplitude during firing pause in (A) and example of positive correlation (*right*) between local spike rate and amplitude during firing cessation. Least squares linear fit indicated in dotted lines following color scheme in (A) with Pearson's correlation coefficient indicated above each plot.

d. Trajectory of unit activity over time during seizure in local spike rate vs spike amplitude space, with increasing time indicated by increasingly lighter copper color. The first time period of firing rate reduction in (A) is indicated with an arrow as "Pause" and the second time period of firing rate reduction is indicated with an arrow as "Cessation."'

e. Summary of observed dynamics in cell-type specific firing rate and inferred membrane potential trajectories.
Blue box: Following seizure onset, some FS cells can stop firing for brief periods (as observed on extracellular electrodes, upper panel). This pause in firing is coupled with signs of hyperpolarization in the inferred membrane potential (lower panel).
Red box: As the seizure starts to transition to a dramatically higher amplitude FS cells stop firing (as observed on extracellular electrodes, upper panel). This cessation is coupled with signs of excessive depolarization in the inferred membrane potential (lower panel; resting membrane potential indicated as dashed line). This is likely due to elevated extracellular potassium ion concentrations by this point of the seizure or increased synaptic drive.
Green box: The subsequent stage of high amplitude spike-and-wave rhythms corresponds to a transient increase and then decrease of firing rate amongst RS cells (as observed on extracellular electrodes, upper panel). This decrease in firing rate is coupled with signs of excessive depolarization in the inferred membrane potential (lower panel).

845 **SUPPLEMENTARY INFORMATION**

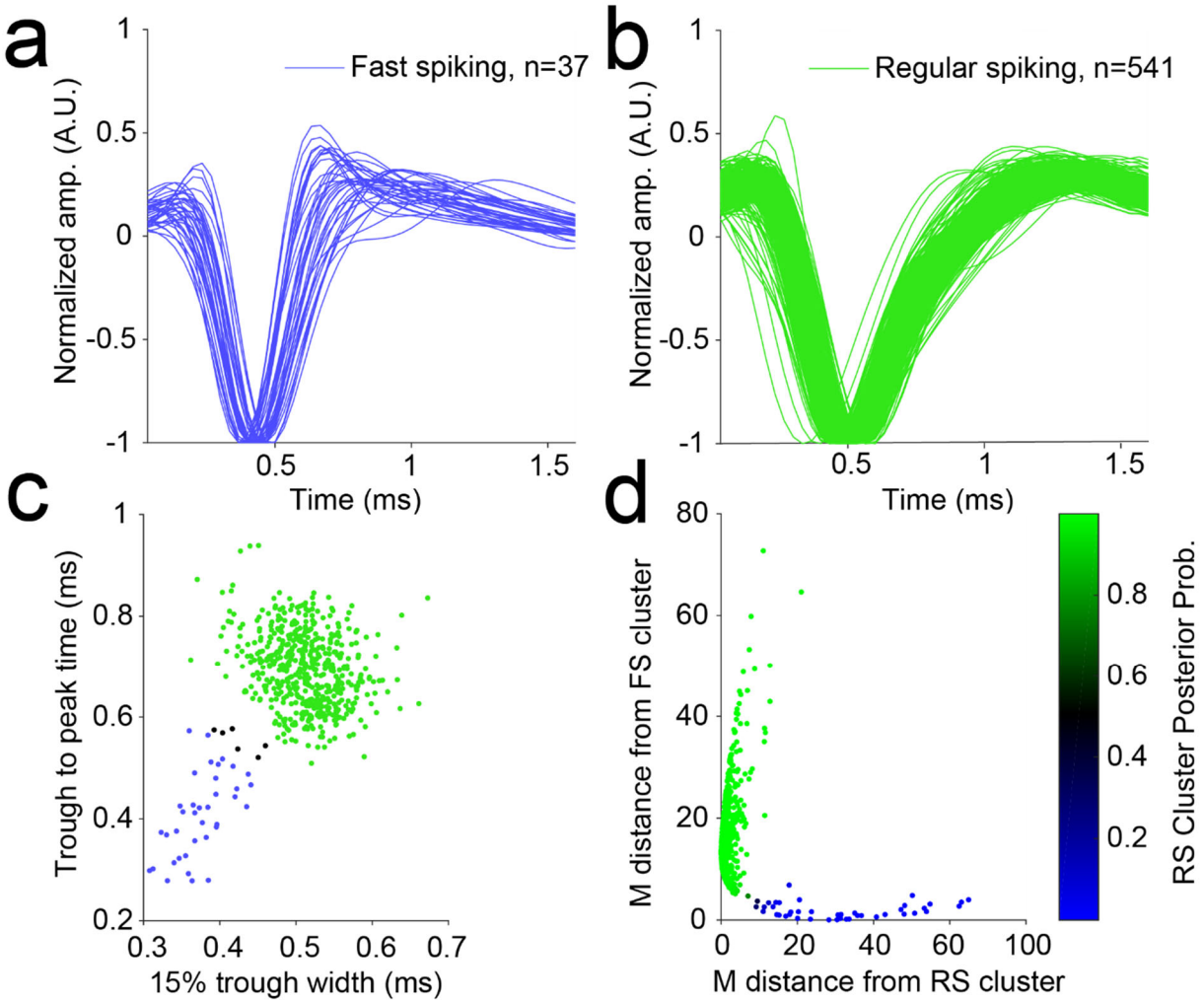

846

847 **Extended Data Figure 1: Human neural activity classification**

848 **a.** Average waveform of each FS-classified unit, normalized by the value the waveform reaches at
849 its trough. The overlaid average waveforms show visual consistency amongst all units classified
850 as FS and as having spike widths narrower than those of RS-classified units.

851 **b.** Average waveform of each RS-classified unit, normalized by the value the waveform reaches at
852 its trough. The overlaid average waveforms show visual consistency amongst all units classified
853 as RS and as having spike widths wider than those of FS-classified units.

854 **c.** All units indicated as points in the average waveform feature space that produced optimal cluster
855 separation, namely the width of the waveform at the potential corresponding to 15% of the
856 potential at its trough and the time between the trough and peak of the waveform. Clustering was
857 automated using a Gaussian Mixture Model where points with posterior probability exceeding
858 0.95 were assigned to the closest centroid. Black dots indicate units that did not exceed this
859 threshold for either Gaussian cloud and were thus unclassified and not used in the remainder of
860 the study.

861 **d.** Mahalanobis distance of each unit from both the RS and FS clusters with color indicating its
862 posterior probability of belonging to the RS cluster. Closeness of points to both axes shows that
863 the clusters are well-separated when accounting for their different variances along different
864 directions in feature space.

865

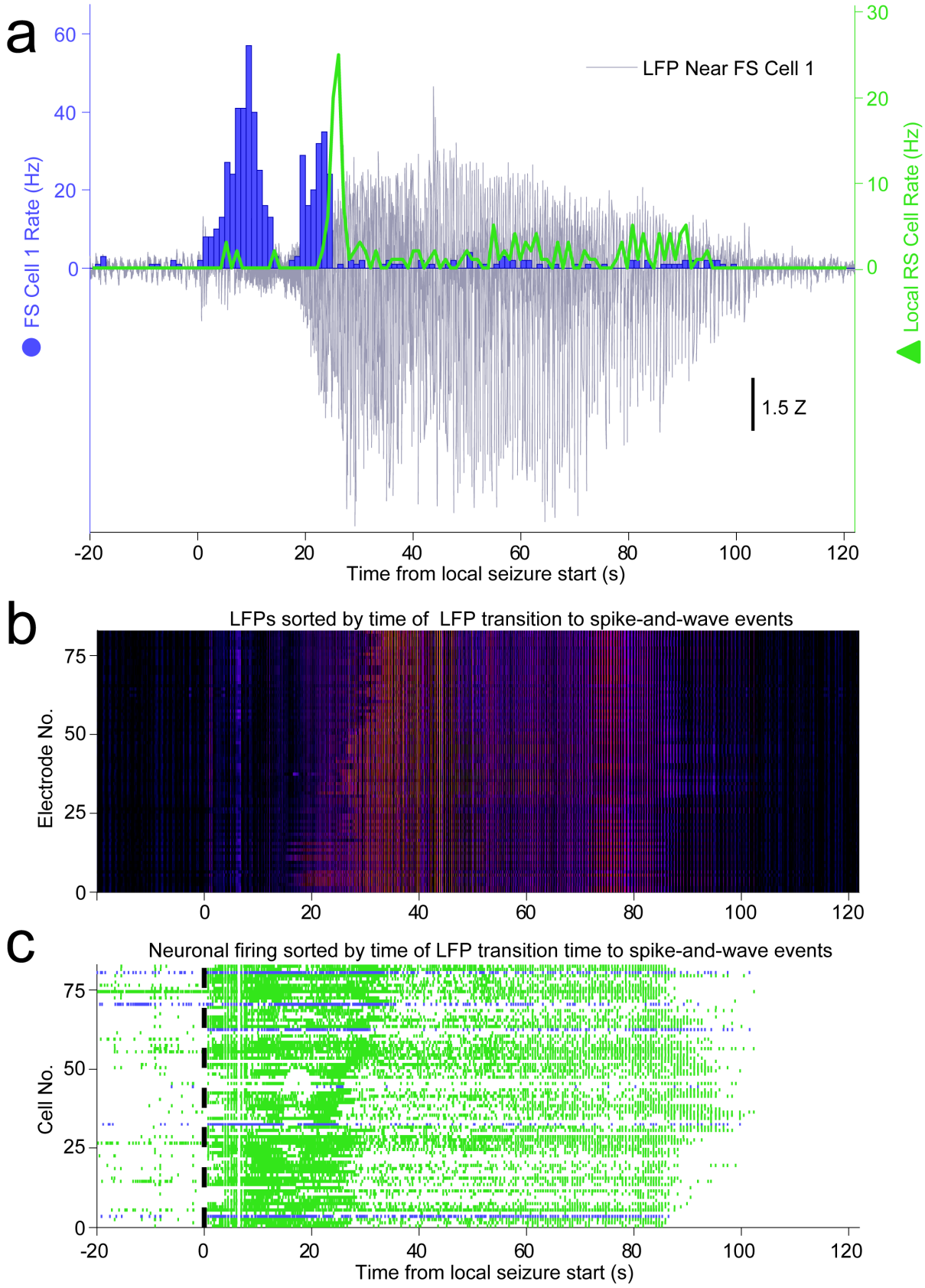
a
LFP Near FS Cell 1
FS Cell 1 Rate (Hz)
Local RS Cell Rate (Hz)
1.5 Z
Time from local seizure start (s)
b
LFPs sorted by time of LFP transition to spike-and-wave events
Electrode No.
c
Neuronal firing sorted by time of LFP transition time to spike-and-wave events
Cell No.
Time from local seizure start (s)

866

867 **Extended Data Figure 2: Human neocortical inhibitory and excitatory neuron activities have**
868 **distinct temporal profiles relative to secondarily generalized focal seizure progression on local**
869 **electrodes, Patient A, Seizure 2**

870 **a.** The LFP (gray) recorded at the same location as FS Cell 1 (blue) dramatically increases at the
871 same time as FS Cell 1 decreases firing. FS Cell 1 activity cessation again precedes a sharp
872 increase in local RS cell activity (green), further suggesting an important role of FS cells in
873 controlling local activity during seizure progression.

874 **b.** Heatmap shows local LFP amplitude (absolute value) over time on each electrode in NeuroPort
875 array exhibiting classifiable units as each row, sorted by time of start of spike-and-wave event
876 and with brighter colors indicating larger amplitudes.

877 **c.** Raster plot showing spike times of all cells on NeuroPort array in Patient B that could be
878 classified into FS (blue) or RS (green) categories with rows sorted by the same order as in (B).
879 Note the increasing delay to reduction in spike density corresponding to LFP transition to spike-
880 and-wave events suggesting control of local seizure progression by local cellular spiking activity.

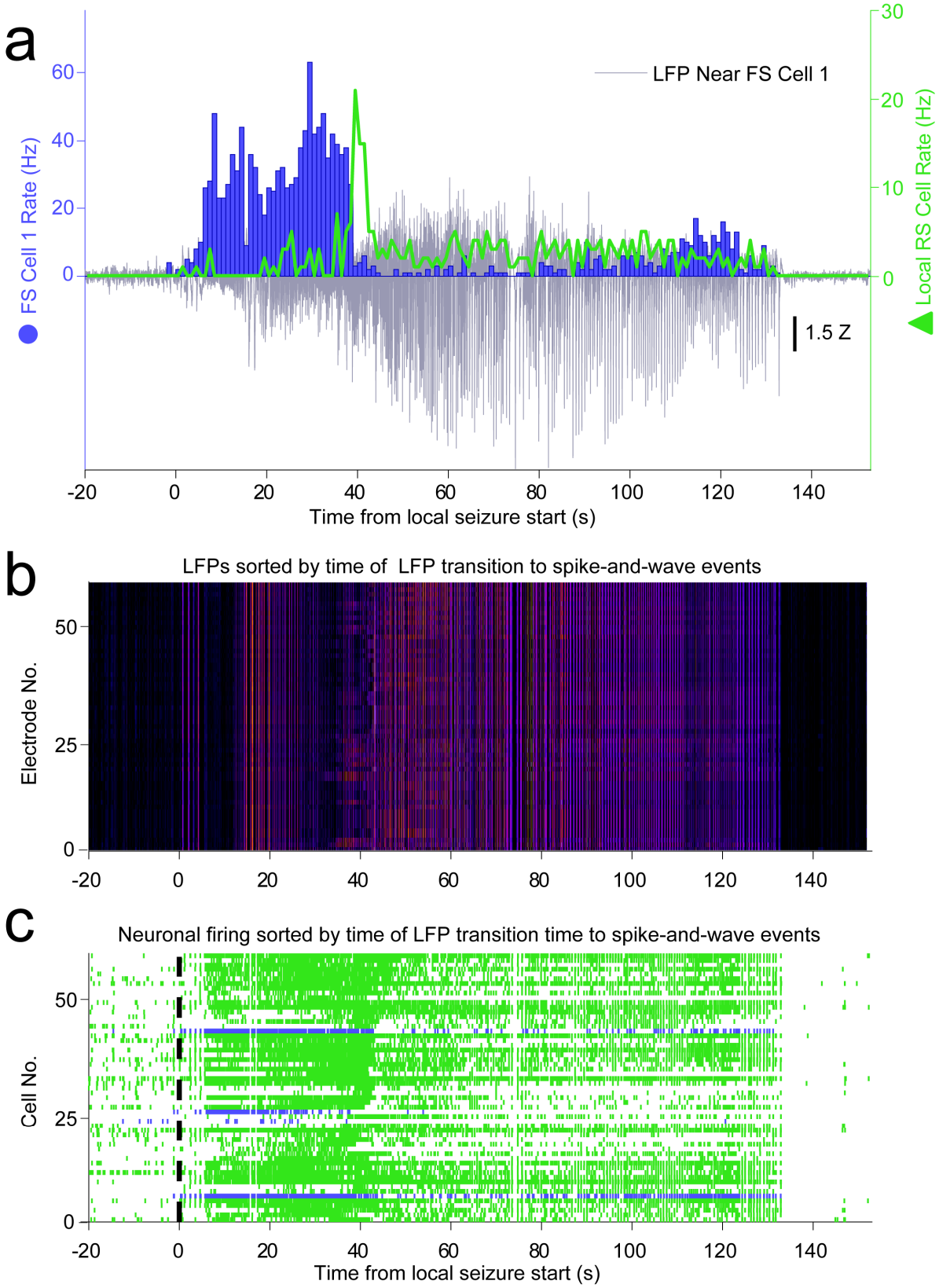
a
LFP Near FS Cell 1
FS Cell 1 Rate (Hz)
Local RS Cell Rate (Hz)
1.5 Z
Time from local seizure start (s)
b
LFPs sorted by time of LFP transition to spike-and-wave events
Electrode No.
c
Neuronal firing sorted by time of LFP transition time to spike-and-wave events
Cell No.
Time from local seizure start (s)

881

Extended Data Figure 3: Human neocortical inhibitory and excitatory neuron activities have distinct temporal profiles relative to secondarily generalized focal seizure progression on local electrodes, Patient C, Seizure 2

- **a.** The LFP (gray) recorded at the same location as FS Cell 1 (blue) dramatically increases at the same time as FS Cell 1 decreases firing. FS Cell 1 activity cessation again precedes a sharp increase in local RS cell activity (green), further suggesting an important role of FS cells in controlling local activity during seizure progression.
- **b.** Heatmap shows local LFP amplitude (absolute value) over time on each electrode in NeuroPort array exhibiting classifiable units as each row, sorted by time of start of spike-and-wave event and with brighter colors indicating larger amplitudes.
- **c.** Raster plot showing spike times of all cells on NeuroPort array in Patient C that could be classified into FS (blue) or RS (green) categories with rows sorted by the same order as in (B). Note the increasing delay to reduction in spike density corresponding to LFP transition to spike-and-wave events suggesting control of local seizure progression by local cellular spiking activity.

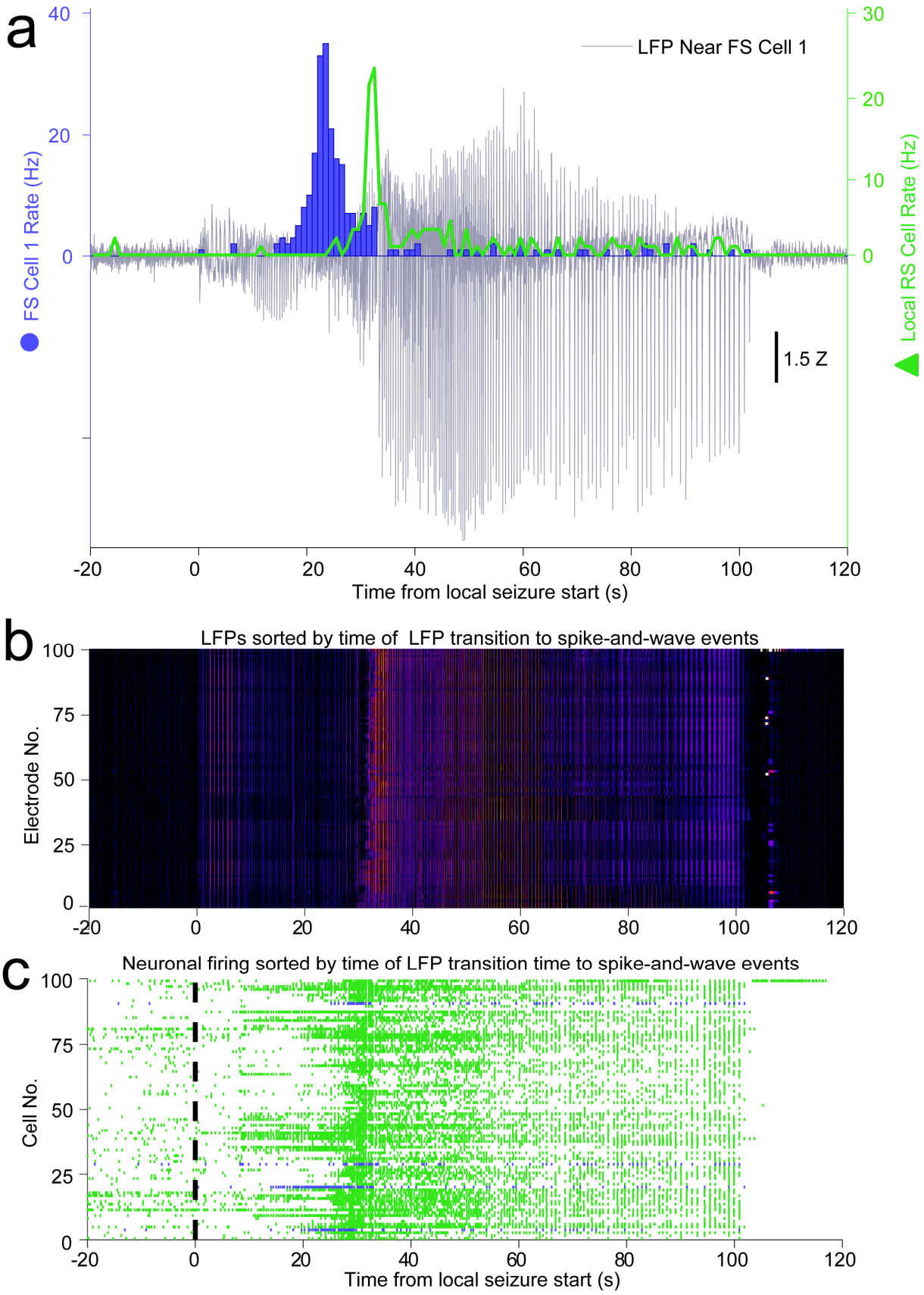
a
LFP Near FS Cell 1
FS Cell 1 Rate (Hz)
Local RS Cell Rate (Hz)
1.5 Z
Time from local seizure start (s)
b
LFPs sorted by time of LFP transition to spike-and-wave events
Electrode No.
c
Neuronal firing sorted by time of LFP transition time to spike-and-wave events
Cell No.
Time from local seizure start (s)

897

898 **Extended Data Figure 4: Human neocortical inhibitory and excitatory neuron activities have**
899 **distinct temporal profiles relative to secondarily generalized focal seizure progression on local**
900 **electrodes, Patient B, Seizure 1**

901 **a.** The LFP (gray) recorded at the same location as FS Cell 1 (blue) dramatically increases at the
902 same time as FS Cell 1 decreases firing. FS Cell 1 activity cessation again precedes a sharp
903 increase in local RS cell activity (green), further suggesting an important role of FS cells in
904 controlling local activity during seizure progression.

905 **b.** Heatmap shows local LFP amplitude (absolute value) over time on each electrode in NeuroPort
906 array exhibiting classifiable units as each row, sorted by time of start of spike-and-wave event
907 and with brighter colors indicating larger amplitudes.

908 **c.** Raster plot showing spike times of all cells on NeuroPort array in Patient C that could be
909 classified into FS (blue) or RS (green) categories with rows sorted by the same order as in (B).

910

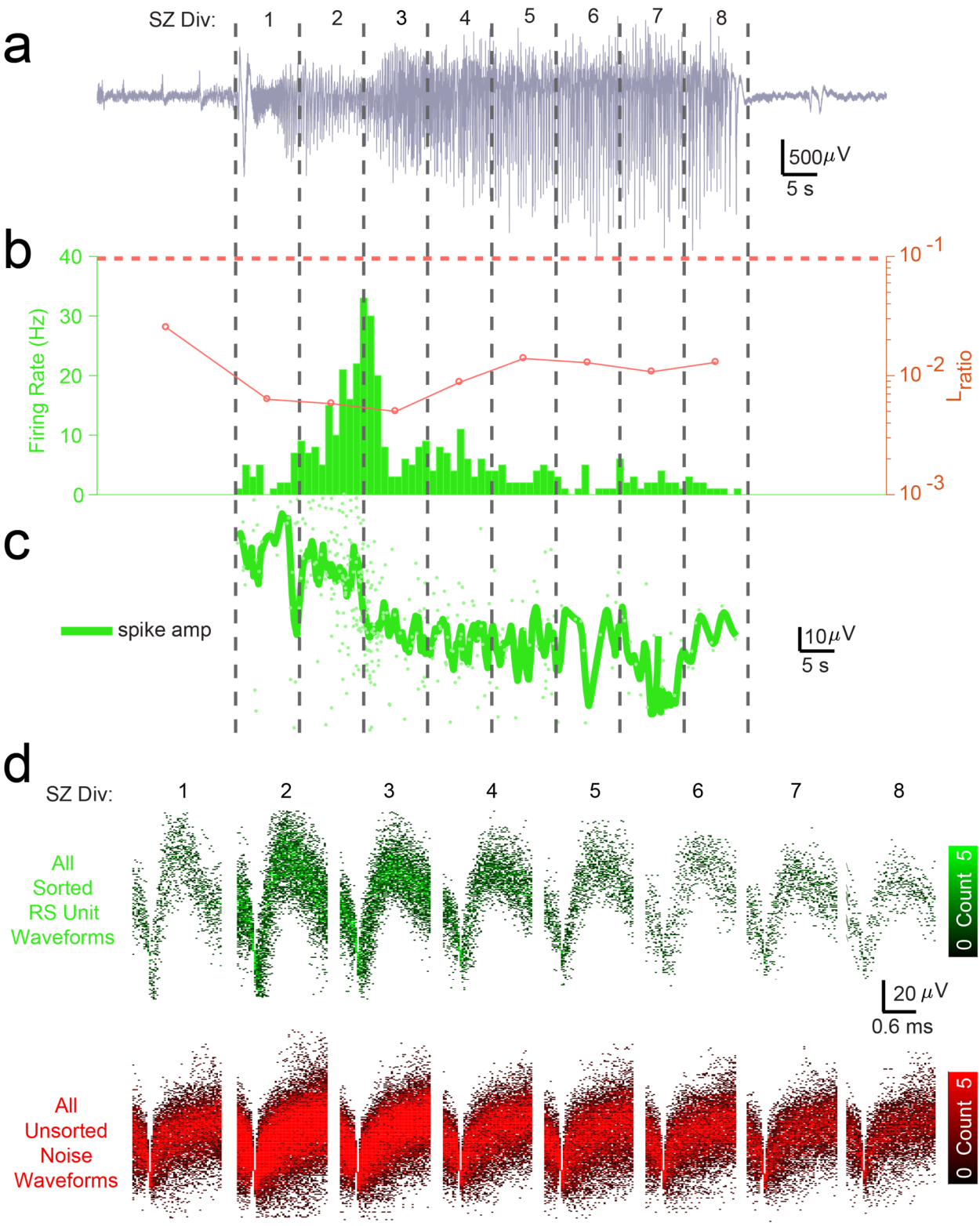

Extended Data Figure 5: Cluster isolation quality assessment suggests RS units are well-isolatable across seizure despite changing unit amplitude and noise structure, allowing analysis of firing rate changes across seizure.

a. LFP in Patient C indicating seizure as split into 8 equal time divisions for analysis of unit isolation quality across duration of seizure.

b. Bar graph shows firing rate in 1 second bins of best-isolated example RS unit (green) in Patient C. Dotted red line indicates threshold used to determine best-isolated units using the dynamic L_{ratio} measure (see Methods) in each time division of seizure. Line plot indicates dynamic L_{ratio} in each division and shows large separation of example FS unit from noise in feature space used for clustering throughout the seizure (note log scale).

c. Line plot showing average spike amplitude (dark green) and individual spike amplitudes (light green) of example RS unit over course of seizure in Patient C. Note that even as amplitude decreases the unit remains well-isolated from noise as quantified by dynamic L_{ratio} across seizure.

d. Time-voltage histogram of all threshold crossings assigned to this example RS unit (green, *Upper)* and to noise (red, *Lower*) in eight divisions of seizure in Patient C. Shows unit waveforms are visually distinguishable from threshold crossings assigned as noise across seizure.

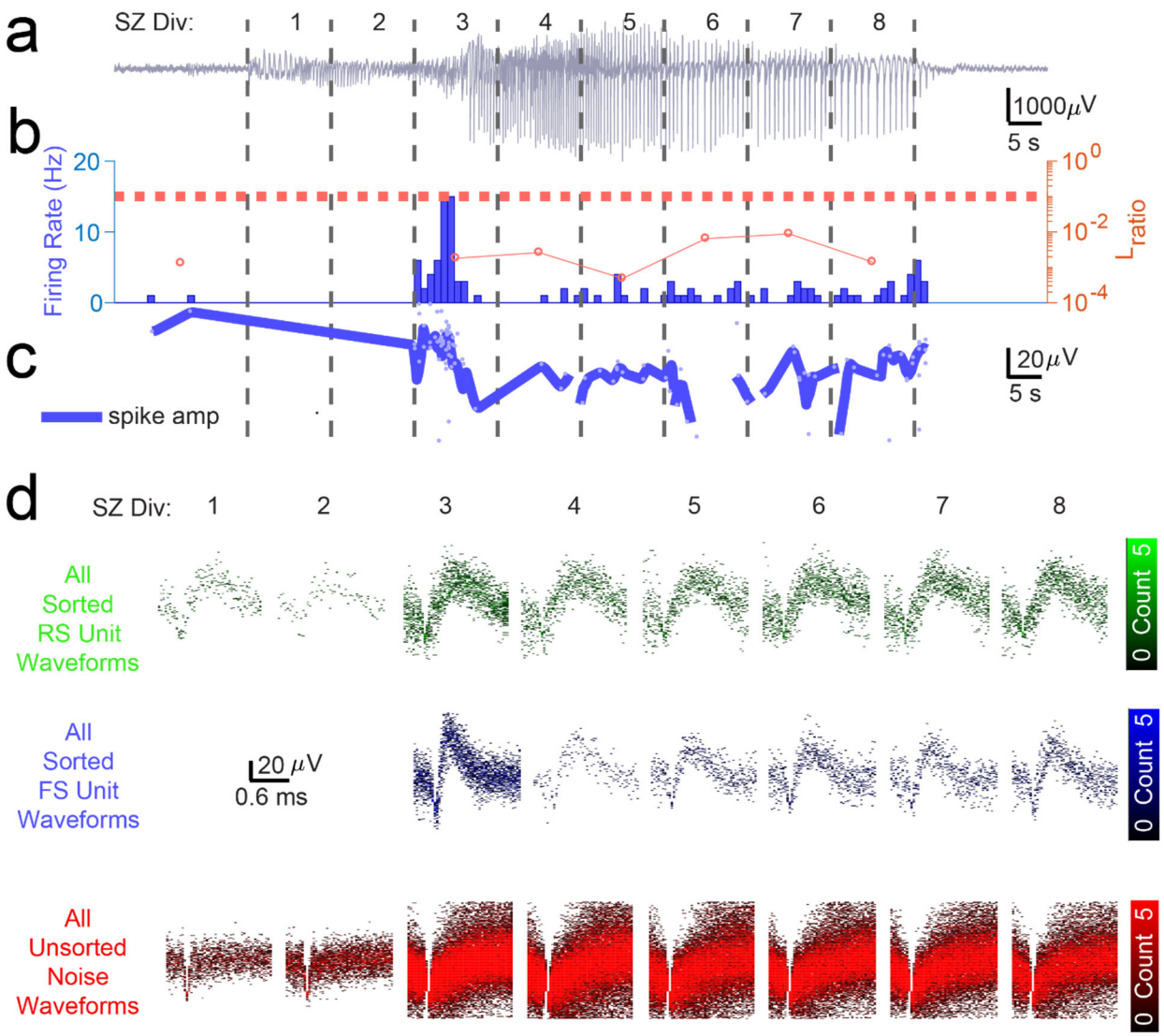
a
SZ Div:
1
2
3
4
5
6
7
8
1000μV
5 s
b
Firing Rate (Hz)
20
10
0
10^0
10^{-2}
10^{-4}
L_{ratio}
c
spike amp
20μV
5 s
d
SZ Div:
1
2
3
4
5
6
7
8
All Sorted RS Unit Waveforms
0 Count 5
All Sorted FS Unit Waveforms
20 μV
0.6 ms
0 Count 5
All Unsorted Noise Waveforms
0 Count 5

935

936 **Extended Data Figure 6: Cluster isolation quality assessment suggests RS and FS units on same**
937 **channel are well-isolatable across seizure despite changing unit amplitude and noise structure,**
938 **allowing analysis of firing rate changes across seizure for multiple patients.**

939 **a.** LFP in Patient B indicating seizure as split into 8 equal time divisions for analysis of unit isolation
940 quality across duration of seizure.

941 **b.** Bar graph shows firing rate in 1 second bins of best-isolated example FS unit (blue) in Patient B.
942 Dotted red line indicates threshold used to determine best-isolated units using the dynamic L_{ratio}
943 measure (see Methods) in each time division of seizure. Line plot indicates dynamic L_{ratio} in each
944 division and shows large separation of example FS unit from noise in feature space used for
945 clustering throughout the seizure (note log scale).

946 **c.** Line plot showing average spike amplitude (dark blue) and individual spike amplitudes (light blue)
947 of example FS unit over course of seizure in Patient B. Note that even as amplitude decreases
948 the unit remains well-isolated from noise as quantified by dynamic L_{ratio} across seizure.

949 **d.** Time-voltage histogram of all threshold crossings assigned to example FS unit (blue, *Middle),* RS
950 unit on same channel (green, *Upper*), and to noise (red, *Lower*) in eight divisions of seizure in
951 Patient B. Shows unit waveforms are visually distinguishable from threshold crossings assigned
952 as noise and as other units across seizure.

953

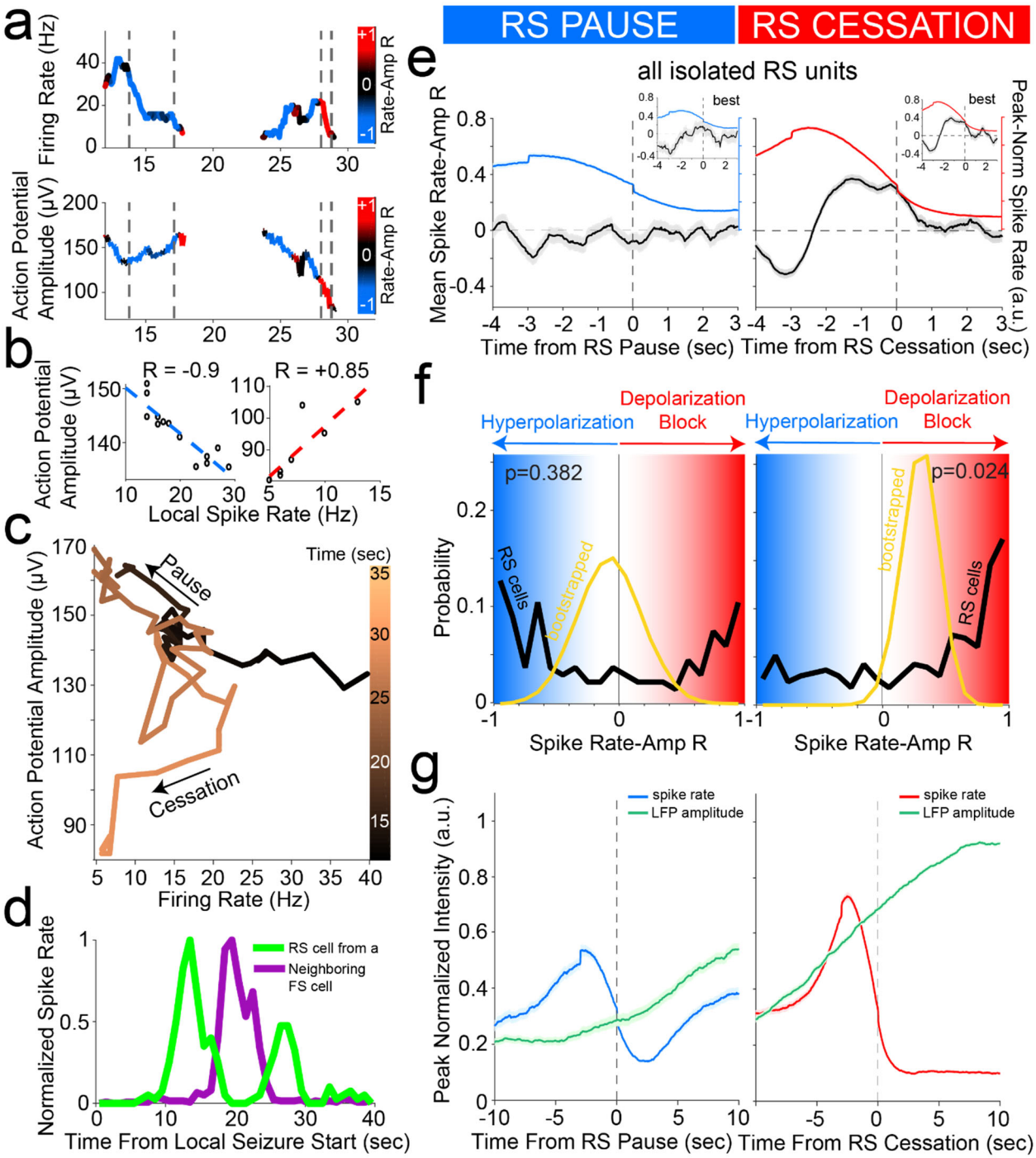

Extended Data Figure 7: Cessation of individual RS unit activity is consistently associated with inferred membrane potential signatures of depolarization block, despite prior pauses

a. Firing rate *(upper)* and trough-to-peak spike amplitude (*lower*) of example RS unit in Patient A, color-coded by the local correlation between spike rate and amplitude (in 1 second time bins) as an extracellular proxy for membrane potential trajectory and subthreshold input history. Dotted lines indicate starts and ends of two time periods of firing rate suppression characterized by different membrane potential signatures further characterized in (B), namely a negative correlation regime corresponding to inhibition followed by a positive correlation regime

963 corresponding to over-excitation ending in firing rate cessation putatively though depolarization
964 block.
965 **b.** Example of negative correlation (*left*) between local spike rate and amplitude in first time period
966 indicated by dotted lines in (A) and example of positive correlation (*right*) between local spike rate
967 and amplitude in second time period indicated by dotted lines in (A). Least squares linear fit
968 indicated in dotted lines following color scheme in (A) with Pearson's correlation coefficient
969 indicated above each plot.
970 **c.** Trajectory of unit activity over time during seizure in local spike rate vs spike amplitude space,
971 with increasing time indicated by increasingly lighter copper color. The first time period of firing
972 rate reduction in dotted lines in (A) is indicated with an arrow as "Pause" and the second time
973 period of firing rate reduction in dotted lines in (A) is indicated with an arrow as "Cessation."
974 **d.** Firing rate of unit from (A) with neighboring FS unit firing rate overlaid, giving further evidence that
975 first period of firing rate suppression corresponds to inhibition from local FS units while second
976 period of firing rate suppression does not correspond to inhibition from local FS units.
977 **e.** Unit cessation-triggered population average of the time course of novel membrane potential
978 regime measure, i.e. the correlation coefficient relating spiking amplitude and rate in a local time
979 window, around the two significant descents in firing rate (below 30% of peak rate) that occur in
980 sequence during seizure. These are designated as pause (*left panel*) and cessation (*right panel*).
981 Left panel shows population average firing rate (blue) and inferred membrane potential regime
982 (black) aligned according to the time of pause in each unit, for all RS units displaying a pause
983 (n=176), with inset showing average for best-isolated RS units displaying a pause (n=41). Right
984 panel shows population average firing rate (red) and inferred membrane potential regime (black)
985 aligned according to the cessation time of each unit, for all RS units meeting cessation criteria
986 (n=379), with inset showing average for best-isolated RS units (n=111).
987 **f.** Probability distribution of membrane potential regime measure (spike rate-amplitude correlation;
988 black line) at the time of pause (*left panel*) for RS unit pausing subpopulation (n=176) with sample
989 mean distribution (gold line; resampling size n=10, $N_{bootstrap}$=50,000) showing a bimodal
990 distribution of correlation coefficients near +1 and -1 , i.e. in the hyperpolarized membrane
991 potential regime (blue) or in the highly depolarized regime (red). The population distribution of
992 inferred membrane potential regime is also shown at the time of cessation (*right panel*) for the RS
993 unit population meeting cessation criteria (n=379) with sample mean distribution (gold line;
994 resampling size n=10, $N_{bootstrap}$=50,000) showing the mean correlation to be significantly above
995 zero, i.e. in the highly depolarized membrane potential regime (red). This is indicative of
996 widespread depolarization block occurring across RS population at the time of cessation.
997 **g.** Unit cessation-triggered population average of the time course of same-electrode LFP amplitude
998 around unit activity pause (*left panel*) and cessation (*right panel*). In particular, left panel shows
999 population average firing rate (blue) and LFP amplitude (black) aligned according to the time of
1000 pause in each unit, for all RS units displaying a pause (n=176). Right panel shows population
1001 average firing rate (red) and LFP amplitude (black) aligned according to the time of cessation in
1002 each unit, for all RS units (n=379).

1003

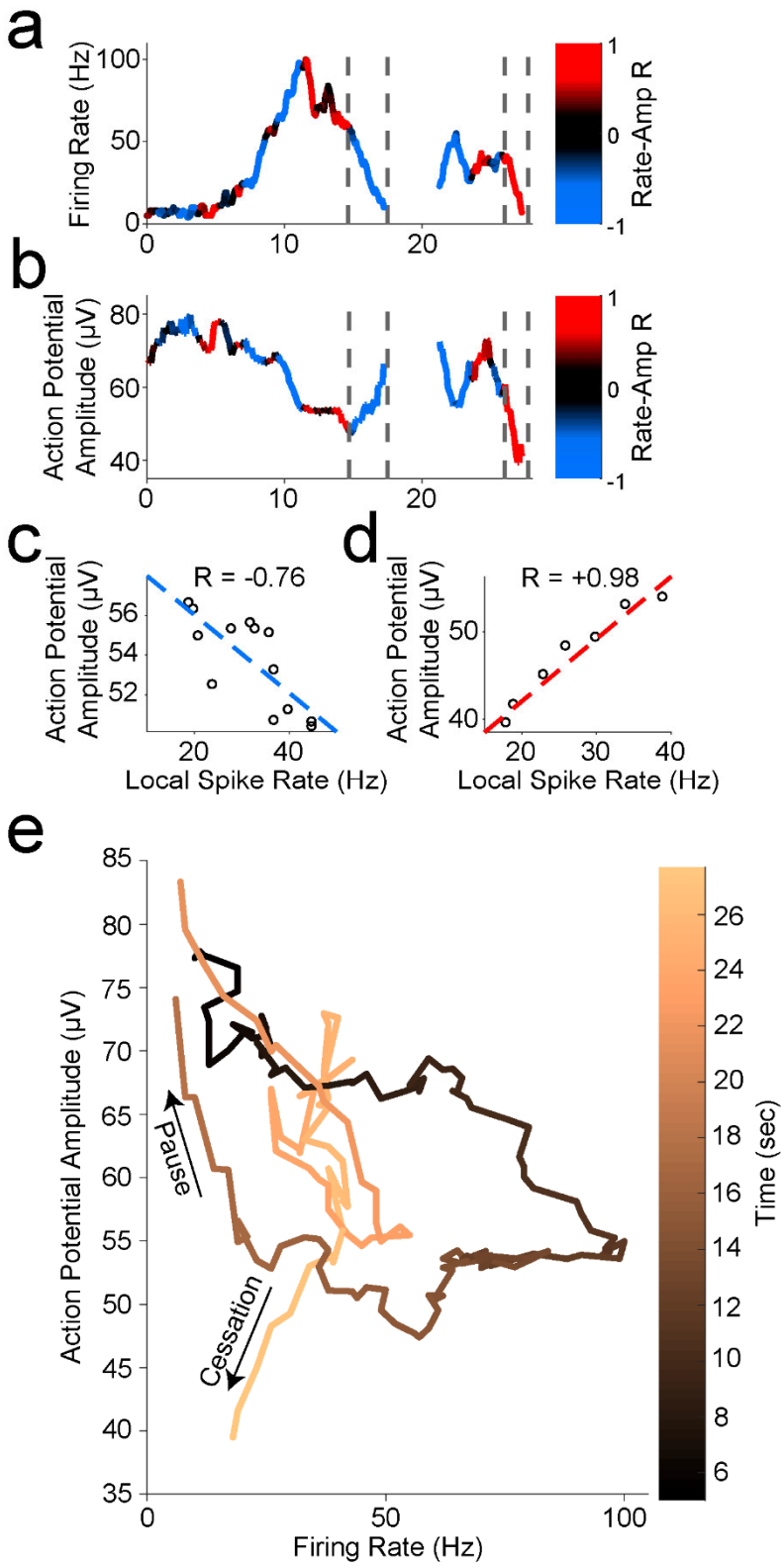
a
Firing Rate (Hz)
100
50
0
0
10
20
1
0
-1
Rate-Amp R
b
Action Potential Amplitude (μV)
80
60
40
0
10
20
1
0
-1
Rate-Amp R
c
Action Potential Amplitude (μV)
R = -0.76
56
54
52
20
40
Local Spike Rate (Hz)
d
Action Potential Amplitude (μV)
R = +0.98
50
40
20
30
40
Local Spike Rate (Hz)
e
Action Potential Amplitude (μV)
85
80
75
70
65
60
55
50
45
40
35
Pause
Cessation
0
50
100
Firing Rate (Hz)
26
24
22
20
18
16
14
12
10
8
6
Time (sec)

1004

Extended Data Figure 8: Seizure progression is consistently associated with extracellular signs of depolarization block preceded by inhibition in single units.

- **a.** Firing rate *(upper)* and trough-to-peak spike amplitude (*lower*) of another example FS unit in Patient A, color-coded by the local correlation between spike rate and amplitude (in 1 second time bins) as an extracellular proxy for membrane potential and subthreshold input history. Dotted lines indicate starts and ends of two time periods of firing rate suppression characterized by different membrane potential signatures further characterized in (B), namely a negative correlation regime corresponding to inhibition followed by a positive correlation regime corresponding to over-excitation ending in firing rate cessation putatively though depolarization block.
- **b.** Example of negative correlation (*left*) between local spike rate and amplitude in first time period indicated by dotted lines in (A) and example of positive correlation (*right*) between local spike rate and amplitude in second time period indicated by dotted lines in (A). Least squares linear fit indicated in dotted lines following color scheme in (A) with Pearson's correlation coefficient indicated above each plot.
- **c.** Trajectory of unit activity over time during seizure in local spike rate vs spike amplitude space, with increasing time indicated by increasingly lighter copper color. The first time period of firing rate reduction in dotted lines in (A) is indicated with an arrow as "Pause" and the second time period of firing rate reduction in dotted lines in (A) is indicated with an arrow as "Cessation."

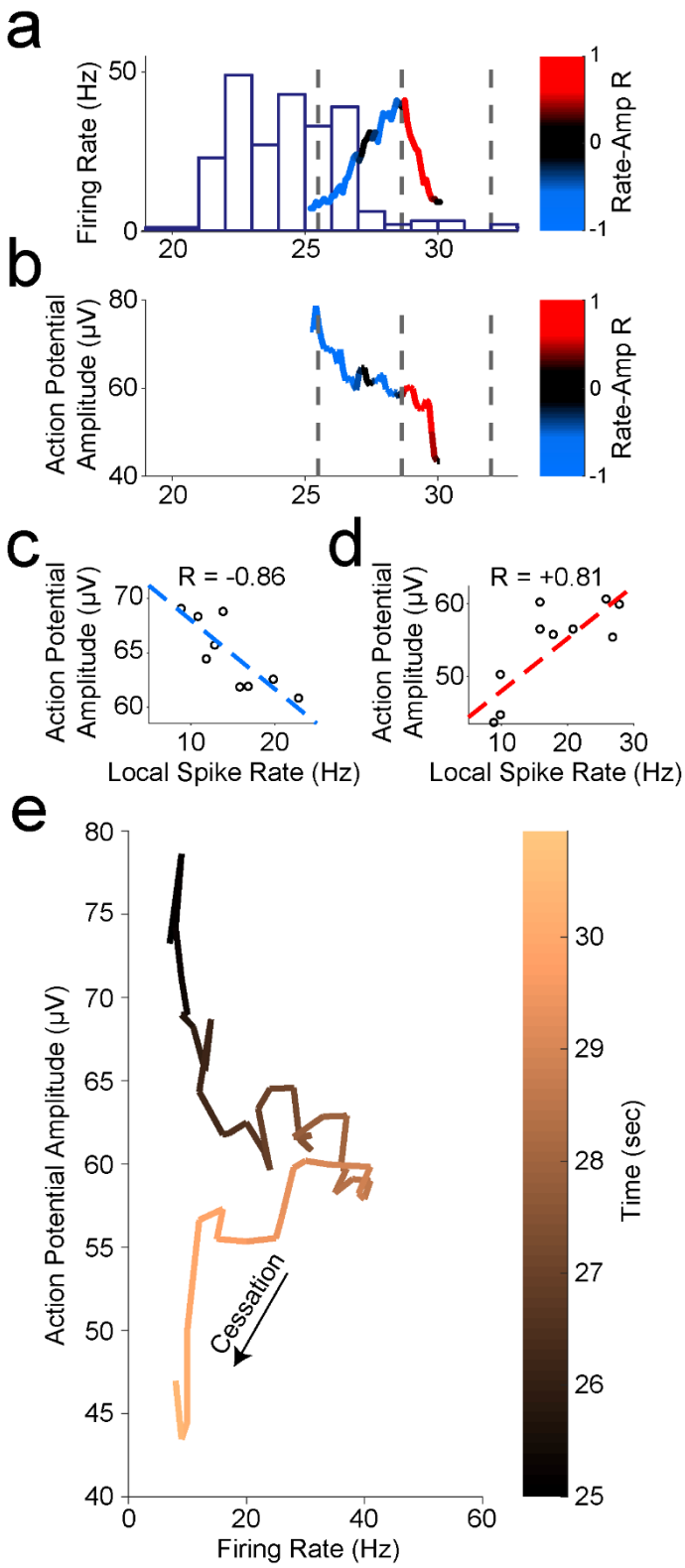
a
Firing Rate (Hz)
50
0
20
25
30
1
0
-1
Rate-Amp R
b
Action Potential Amplitude (μV)
80
60
40
20
25
30
1
0
-1
Rate-Amp R
c
R = -0.86
Action Potential Amplitude (μV)
70
65
60
10
20
Local Spike Rate (Hz)
d
R = +0.81
Action Potential Amplitude (μV)
60
50
10
20
30
Local Spike Rate (Hz)
e
Action Potential Amplitude (μV)
80
75
70
65
60
55
50
45
40
0
20
40
60
Firing Rate (Hz)
Cessation
30
29
28
27
26
25
Time (sec)

1025

Extended Data Figure 9: Seizure progression is consistently associated with extracellular signs of depolarization block preceded by inhibition in single units.

a. Firing rate *(upper)* and trough-to-peak spike amplitude (*lower*) of another example RS unit in Patient A, color-coded by the local correlation between spike rate and amplitude (in 1 second time bins) as an extracellular proxy for membrane potential and subthreshold input history. Firing rate of local FS unit is overlaid as purple histogram. Dotted lines indicate start and end times of two time periods of firing rate suppression characterized by different membrane potential signatures further characterized in (B), namely a negative correlation regime corresponding to inhibition followed by a positive correlation regime corresponding to over-excitation ending in firing rate cessation putatively though depolarization block.

b. Example of negative correlation (*left*) between local spike rate and amplitude in first time period indicated by dotted lines in (A) and example of positive correlation (*right*) between local spike rate and amplitude in second time period indicated by dotted lines in (A). Least squares linear fit indicated in dotted lines following color scheme in (A) with Pearson's correlation coefficient indicated above each plot.

c. Trajectory of unit activity over time during seizure in local spike rate vs spike amplitude space, with increasing time indicated by increasingly lighter copper color. RS unit is released from inhibition shortly following the cessation of activity in local FS unit as indicated by increasing firing rate with decreasing amplitude but then enters regime of over-excitation indicated by decreasing firing rate with decreasing amplitude at trajectory "corner" corresponding to a spiking rate of 40 Hz, until the unit ceases to fire likely due to depolarization block given these indicators of membrane potential history.

1062

1063 **REFERENCES**

1064

1065 1. Annegers, J. F. The Treatment of Epilepsy: Principles and Practice. (Third
1066 Edition). in *The Treatment of Epilepsy: Principles and PRac* (ed. Wyllie, E.) 131–
1067 138 (Wiley, 2001). doi:10.1002/hup.372
1068 2. Thurman, D. J. *et al.* Standards for epidemiologic studies and surveillance of
1069 epilepsy. *Epilepsia* **52**, 2–26 (2011).
1070 3. Žiburkus, J., Cressman, J. R. & Schiff, S. J. Seizures as imbalanced up states:
1071 excitatory and inhibitory conductances during seizure-like events. *J. Neurophysiol.*
1072 **109**, 1296–1306 (2013).
1073 4. Farrell, J. S., Nguyen, Q.-A. & Soltesz, I. Review Resolving the Micro-Macro
1074 Disconnect to Address Core Features of Seizure Networks. *Neuron* **101**, 1016–
1075 1028 (2019).
1076 5. Elahian, B. *et al.* Low-voltage fast seizures in humans begin with increased
1077 interneuron firing. *Ann. Neurol.* **84**, 588–600 (2018).
1078 6. Weiss, S. A. *et al.* Ictal onset patterns of local field potentials, high frequency
1079 oscillations, and unit activity in human mesial temporal lobe epilepsy. *Epilepsia*
1080 **57**, 111–121 (2016).
1081 7. Schwartzkroin, P. A. & Prince, D. A. Changes in excitatory and inhibitory synaptic
1082 potentials leading to epileptogenic activity. *Brain Res.* **183**, 61–77 (1980).
1083 8. Gutnick, M. J., Connors, B. W. & Prince, D. A. Mechanisms of neocortical
1084 epileptogenesis in vitro. *J. Neurophysiol.* **48**, 1321–1335 (1982).
1085 9. Prince, D. A. & Connors, B. W. Mechanisms of epileptogenesis in cortical
1086 structures. *Ann. Neurol.* **16**, S59–S64 (1984).
1087 10. McCormick, D. A., Connors, B. W., Lighthall, J. W. & Prince, D. A. Comparative
1088 electrophysiology of pyramidal and sparsely spiny stellate neurons of the
1089 neocortex. *J. Neurophysiol.* **54**, 782–806 (1985).
1090 11. Chagnac-Amitai, Y. & Connors, B. W. Horizontal spread of synchronized activity
1091 in neocortex and its control by GABA-mediated inhibition. *J. Neurophysiol.* **61**,
1092 747–758 (1989).
1093 12. Ziburkus, J., Cressman, J. R., Barreto, E. & Schiff, S. J. Interneuron and
1094 pyramidal cell interplay during in vitro seizure-like events. *J. Neurophysiol.* **95**,
1095 3948–3954 (2006).
1096 13. Trevelyan, A. J. & Schevon, C. A. How inhibition influences seizure propagation.
1097 *Neuropharmacology* **69**, 45–54 (2013).
1098 14. Karlócai, M. R. *et al.* Physiological sharp wave-ripples and interictal events in
1099 vitro: what's the difference? *Brain* **137**, 463–85 (2014).
1100 15. Pavlov, I. & Walker, M. C. Tonic GABAA receptor-mediated signalling in temporal
1101 lobe epilepsy. *Neuropharmacology* **69**, 55–61 (2013).
1102 16. Avoli, M. & de Curtis, M. GABAergic synchronization in the limbic system and its
1103 role in the generation of epileptiform activity. *Progress in Neurobiology* **95**, 104–
1104 132 (2011).
1105 17. Cope, D. W. *et al.* Enhanced tonic GABA A inhibition in typical absence epilepsy.
1106 *Nat. Med.* **15**, 1392–1398 (2009).

1107 18. Neumann, A. R. *et al.* Involvement of fast-spiking cells in ictal sequences during
1108 spontaneous seizures in rats with chronic temporal lobe epilepsy. *Brain* **140**,
1109 2355–2369 (2017).
1110 19. Sessolo, M. *et al.* Parvalbumin-positive inhibitory interneurons oppose
1111 propagation but favor generation of focal epileptiform activity. *J. Neurosci.* **35**,
1112 9544–9557 (2015).
1113 20. Lévesque, M., Herrington, R., Hamidi, S. & Avoli, M. Interneurons spark seizure-
1114 like activity in the entorhinal cortex. *Neurobiol. Dis.* **87**, 91–101 (2016).
1115 21. Khoshkhoo, S., Vogt, D. & Sohal, V. S. Dynamic, Cell-Type-Specific Roles for
1116 GABAergic Interneurons in a Mouse Model of Optogenetically Inducible Seizures.
1117 *Neuron* **93**, 291–298 (2017).
1118 22. Xu, H., Jeong, H. Y., Tremblay, R. & Rudy, B. Neocortical Somatostatin-
1119 Expressing GABAergic Interneurons Disinhibit the Thalamorecipient Layer 4.
1120 *Neuron* **77**, 155–167 (2013).
1121 23. Buckmaster, P. S., Jongen-Rêlo, A. L., Davari, S. B. & Wong, E. H. Testing the
1122 disinhibition hypothesis of epileptogenesis in vivo and during spontaneous
1123 seizures. *J. Neurosci.* **20**, 6232–40 (2000).
1124 24. Miri, M. L., Vinck, M., Pant, R. & Cardin, J. A. Altered hippocampal interneuron
1125 activity precedes ictal onset. *Elife* **7**, (2018).
1126 25. Cammarota, M., Losi, G., Chiavegato, A., Zonta, M. & Carmignoto, G. Fast
1127 spiking interneuron control of seizure propagation in a cortical slice model of focal
1128 epilepsy. *J. Physiol.* **591**, 807–822 (2013).
1129 26. Petersen, C. C. H. Whole-Cell Recording of Neuronal Membrane Potential during
1130 Behavior. *Neuron* **95**, 1266–1281 (2017).
1131 27. Nowak, L. G., Azouz, R., Sanchez-Vives, M. V., Gray, C. M. & McCormick, D. A.
1132 Electrophysiological classes of cat primary visual cortical neurons in vivo as
1133 revealed by quantitative analyses. *J. Neurophysiol.* **89**, 1541–1566 (2003).
1134 28. Cardin, J. A. *et al.* Driving fast-spiking cells induces gamma rhythm and controls
1135 sensory responses. *Nature* **459**, 663–667 (2009).
1136 29. Rudy, B., Fishell, G., Lee, S. H. & Hjerling-Leffler, J. Three groups of interneurons
1137 account for nearly 100% of neocortical GABAergic neurons. *Dev. Neurobiol.* **71**,
1138 45–61 (2011).
1139 30. Connors, B. W., Pinto, D. J. & Telfeian, A. E. Local pathways of seizure
1140 propagation in neocortex. *Int. Rev. Neurobiol.* **45**, 527–46 (2001).
1141 31. Merricks, E. M. *et al.* Single unit action potentials in humans and the effect of
1142 seizure activity. *Brain* **138**, 2891–906 (2015).
1143 32. Schevon, C. A. *et al.* Evidence of an inhibitory restraint of seizure activity in
1144 humans. *Nat. Commun.* **3**, 1060 (2012).
1145 33. Sabolek, H. R. *et al.* A candidate mechanism underlying the variance of interictal
1146 spike propagation. *J. Neurosci.* **32**, 3009–3021 (2012).
1147 34. Chervin, R. D., Pierce, P. A. & Connors, B. W. Periodicity and directionality in the
1148 propagation of epileptiform discharges across neocortex. *J. Neurophysiol.* **60**,
1149 1695–1713 (1988).
1150 35. Wong, B. Y. & Prince, D. A. The lateral spread of ictal discharges in neocortical
1151 brain slices. *Epilepsy Res.* **7**, 29–39
1152 36. Golomb, D. & Amitai, Y. Propagating neuronal discharges in neocortical slices:

1153 Computational and experimental study. *J. Neurophysiol.* **78**, 1199–1211 (1997).
1154 37. Liou, J. Y. *et al.* A model for focal seizure onset, propagation, evolution, and
1155 progression. *Elife* **9**, (2020).
1156 38. Martina, M., Schultz, J. H., Ehmke, H., Monyer, H. & Jonas, P. Functional and
1157 molecular differences between voltage-gated K+ channels of fast-spiking
1158 interneurons and pyramidal neurons of rat hippocampus. *J. Neurosci.* **18**, 8111–
1159 8125 (1998).
1160 39. Rudy, B. & McBain, C. J. Kv3 channels: Voltage-gated K+ channels designed for
1161 high-frequency repetitive firing. *Trends in Neurosciences* **24**, 517–526 (2001).
1162 40. Lien, C. C. & Jonas, P. Kv3 potassium conductance is necessary and kinetically
1163 optimized for high-frequency action potential generation in hippocampal
1164 interneurons. *J. Neurosci.* **23**, 2058–2068 (2003).
1165 41. Somjen, G. G. *Ions in the brain : normal function, seizures, and stroke*. (Oxford
1166 University Press, 2004).
1167 42. Fröhlich, F., Bazhenov, M., Iragui-Madoz, V. & Sejnowski, T. J. Reviews:
1168 Potassium dynamics in the epileptic cortex: New insights on an old topic.
1169 *Neuroscientist* **14**, 422–433 (2008).
1170 43. Cruikshank, S. J., Lewis, T. J. & Connors, B. W. Synaptic basis for intense
1171 thalamocortical activation of feedforward inhibitory cells in neocortex. *Nat.*
1172 *Neurosci.* **10**, 462–468 (2007).
1173 44. Pouille, F. & Scanziani, M. Routing of spike series by dynamic circuits in the
1174 hippocampus. *Nature* **429**, 717–723 (2004).
1175 45. Markram, H. *et al.* Interneurons of the neocortical inhibitory system. *Nature*
1176 *Reviews Neuroscience* **5**, 793–807 (2004).
1177 46. Kawaguchi, Y. Physiological subgroups of nonpyramidal cells with specific
1178 morphological characteristics in layer II/III of rat frontal cortex. *J. Neurosci.* **15**,
1179 2638–2655 (1995).
1180 47. Kramer, M. A. *et al.* Human seizures self-terminate across spatial scales via a
1181 critical transition. *Proc. Natl. Acad. Sci. U. S. A.* **109**, 21116–21121 (2012).
1182 48. Beverlin, B., Kakalios, J., Nykamp, D. & Netoff, T. I. Dynamical changes in
1183 neurons during seizures determine tonic to clonic shift. *J. Comput. Neurosci.* **33**,
1184 41–51 (2012).
1185 49. Fröhlich, F., Sejnowski, T. J. & Bazhenov, M. Network bistability mediates
1186 spontaneous transitions between normal and pathological brain states. *J.*
1187 *Neurosci.* **30**, 10734–10743 (2010).
1188 50. Blumenfeld, H. Cellular and network mechanisms of spike-wave seizures.
1189 *Epilepsia* **46**, 21–33 (2005).
1190 51. Berényi, A., Belluscio, M., Mao, D. & Buzsáki, G. Closed-loop control of epilepsy
1191 by transcranial electrical stimulation. *Science (80-.).* **337**, 735–737 (2012).
1192 52. Wykes, R. C. *et al.* Epilepsy: Optogenetic and potassium channel gene therapy in
1193 a rodent model of focal neocortical epilepsy. *Sci. Transl. Med.* **4**, (2012).
1194 53. Paz, J. T. *et al.* Closed-loop optogenetic control of thalamus as a tool for
1195 interrupting seizures after cortical injury. *Nat. Neurosci.* **16**, 64–70 (2013).
1196 54. Krook-Magnuson, E., Armstrong, C., Oijala, M. & Soltesz, I. On-demand
1197 optogenetic control of spontaneous seizures in temporal lobe epilepsy. *Nat.*
1198 *Commun.* **4**, 1–8 (2013).

55. Sukhotinsky, I. *et al.* Optogenetic Delay of Status Epilepticus Onset in an In Vivo Rodent Epilepsy Model. *PLoS One* **8**, (2013).
56. Bikson, M., Hahn, P. J., Fox, J. E. & Jefferys, J. G. R. Depolarization block of neurons during maintenance of electrographic seizures. *J. Neurophysiol.* **90**, 2402–2408 (2003).
57. Hoffman, D. A., Magee, J. C., Colbert, C. M. & Johnston, D. K+ channel regulation of signal propagation in dendrites of hippocampal pyramidal neurons. *Nature* **387**, 869–875 (1997).
58. Schmitzer-Torbert, N., Jackson, J., Henze, D., Harris, K., & Redish, A. D. Quantitative measures of cluster quality for use in extracellular recordings. *Neuroscience* **131**, 1-11 (2005).
59. Magloire, V., Mercier, M. S., Kullmann, D. M., & Pavlov, I. GABAergic interneurons in seizures: Investigating causality with optogenetics. *The Neuroscientist* **25**, 344-358 (2019).
60. De Polavieja, G. G., Harsch, A., Kleppe, I., Robinson, H. P. C. & Juusola, M. Stimulus history reliably shapes action potential waveforms of cortical neurons. *J. Neurosci.* **25**, 5657–5665 (2005).